Structural behaviour of stainless steel beam-to-tubular column joints

Elflah, Mohamed; Theofanous, Marios; Dirar, Samir; Yuan, Huanxin

[Link to publication on Research at Birmingham portal](#)

Structural behaviour of stainless steel beam-to-tubular column joints

Mohamed Elflah[a], Marios Theofanous[a], Samir Dirar[a], Huanxin Yuan[b]*

[a] *Department of Civil Engineering, University of Birmingham, Birmingham B15 2TT, United Kingdom*

[b] *School of Civil Engineering, Wuhan University, Wuhan 430072, PR China*

[*]corresponding author:

Dr Marios Theofanous, *Department of Civil Engineering, University of Birmingham, Birmingham B15 2TT, UK*
 Email: m.theofanous@bham.ac.uk

Abstract

This paper complements previous research conducted by the authors on stainless steel bolted joints and reports the first systematic study on the structural behaviour of stainless steel beam-to-tubular column joints with the use of Hollo-bolts. Six full scale specimens including two flush plate joints, two top and seat cleat connections, and two top, seat and web cleat connections of single-sided beam-to- hollow section column joints have been tested and the results are reported in detail. All specimens were in Grade EN 1.4301 austenitic stainless steel and were designed in such a way that a variety of failure modes could be obtained including plastification of the tubular column face, of the connecting angle cleats or the flush plates. For each specimen the moment-rotation response, the evolution of strains in critical locations of the connections and the separation between the column face and the connected beam was monitored and is reported herein. In parallel with the tests, advanced nonlinear FE models were developed. Following validation against the obtained experimental results, parametric studies were conducted to study the effect of key parameters such as, material grade, column face thickness, end plate/angle cleat thickness and bolt spacing on the stiffness, strength and ductility of the joints. Based on both the experimental and numerical results, it was verified that the connections displayed excellent ductility and attained loads much higher than the ones predicted by design standards for carbon steel joints.

Keywords

Stainless steel joints, beam-to-tubular-column joints, Eurocode 3, Experimental tests, Hollo-bolts

1   Introduction

Tubular structural members are a major area of interest within the field of steel and stainless steel structures and are preferred by many architects due to their aesthetic appeal [1]. In addition to the

traditional family of Square, Rectangular and Circular Hollow Sections (SHS, RHS, CHS), Elliptical Hollow Sections (EHS) are available in both carbon [2] and stainless steel [3]. Among the advantages of hollow section members are their high stiffness about both principal axes, which makes them an attractive choice for compression members and their high torsional stiffness, which makes them efficient to resist torsion and lateral torsional buckling. Moreover, filling the tubular columns with concrete thereby creating composite columns (concrete filled tubes) possessing high strength, stiffness and ductility is an additional potential benefit [4, 5]. However, the closed nature of either bare steel or concrete filled tubular columns complicates the assembly of bolted connections, since hollow section columns allow access only from one side.

Several connection configurations for beam to tubular column joints employing angle cleats, fin plates and T-sections welded on the column face and bolted to the beam have been experimentally investigated [6-8]. It was demonstrated [8] that the minimum thickness of the column face should be related to the thickness of the fin plate to induce yielding of the fin plate prior to failure of the column face by punching shear. An alternative solution involving threaded studs welded to the tubular column was investigated by Maquoi et al. [9]. In addition to the low ductility exhibited by these connections, possible damage of the welded studs during transportation of the columns made this technique less favourable for practical applications [10]. More recently, Málaga-Chuquitaype and Elghazouli [11 conducted tests on and derived a component characterization for bolted connections utilising a reverse channel section welded on the tubular column face and concluded that this joint configuration possesses high ductility, but its strength and stiffness are adversely affected by the strength and stiffness of the channel section. The use of strengthening measures in the form of external diaphragm plates (i.e. collars) welded to concrete filled CHS or SHS was experimentally and numerically investigated [12, 13], whilst the response of joint configurations involving the use of through plates and stiffeners has also been studied [14, 15] for both empty and concrete filled tubular columns. The use of through section beam joints, where slots with the

shape of the beam section are made on the column to allow the connected beam to pass through has also been explored for concrete filled tubular columns [16]. Other less fabrication-intensive connection details have also been explored involving various bolting techniques. A conceptually simple bolted connection involving bolts long enough to go through the column section has been experimentally investigated by Hoang et al. [17] for concrete filled SHS. However, the resulting connection detail is difficult to execute on site and could induce additional cost.

The use of bolted connections on site is desirable provided that the resulting details are easy to execute on site and result in good structural performance. To this end various types of the so-called blind-bolted connections allowing bolted connections to be assembled without requiring access to both sides of the bolts have been developed. A review on past research on various types of blind-bolted connections can be found in [11, 18]. Among the various types of available fasteners for the execution of blind-bolted connections, the use of Hollo-bolts is considered in the present study, as Hollo-bolts are readily available in stainless steel and they have been widely researched both experimentally and numerically. The response of the Hollo-bolt in tension as well as the strength and stiffness of T-stubs employing Hollo-bolts was numerically investigated by Wang et al. [19], who developed an analytical predictive model. Elghazouli et al. [18] studied the behaviour of top and bottom seated angle cleat connection employing different grades and configurations of Hollo-bolts under monotonic and cyclic loading. The results of this study indicated that the bolt configuration affected the behaviour of the studied connections in terms of obtained failure modes, strength and stiffness. A similar series of experiments and numerical simulations was conducted to investigate the response of open beam to tubular column connections under predominantly shear [20] or axial [21] loads. The findings suggest that in general the angle dimensions and the thickness of the column face significantly affect the response characteristics. Design equations for the strength and stiffness of both the Hollo-bolt and the column face in bending according to the component-based approach were developed by Málaga-

Chuquitaype and Elghazouli [22]. Wang and Wang [23] conducted a series of experimental and numerical studies on T-stubs bolted on SHS with Hollo-bolts subjected to tension, thus idealising the response of the tension region of a moment resisting connection. Moreover, they gave a comprehensive overview and assessed the accuracy of relevant design methods for the prediction of the strength of the column face of a tubular column in bending [24-26]. Additional research aiming to improve the performance of blind-bolted joints led to the development of the Extended Hollobolt (EHB), specifically designed for concrete infilled columns [5, 27, 28], as the bolt extension provides an anchor in the concrete leading to the bolt developing its full tensile strength as opposed to the alternative where the blind bolt pulls out prematurely.

All of the aforementioned studies have exclusively dealt with conventional carbon steel joints. Research on stainless steel joints is very limited, even though the high ductility and significant high strain-hardening of stainless steel is expected to significantly affect their strength and overall response. Experimental research on stainless steel joints has primarily focused on bolted and welded lap joints at room temperature [29] as well as at elevated temperatures [30,31]. Departing from studies on simple lap joints, Feng and Young have extensively investigated the structural behaviour, fatigue and failure modes of welded connections between empty and concrete filled stainless steel tubular (RHS/SHS) members representative of typical truss joints between the chord and diagonal members [32-35].

An attempt to study numerically the response of top and seat cleat stainless steel beam-to-column joints was recently reported by Hasan et al. [36], however, the validation of their model was based on existing carbon steel experimental results, and unverified assumptions regarding the material response and the interaction of the various stainless steel components. Elflah et al. [37] reported the only available experimental study to date on stainless steel beam-to-column joints, which they complemented a comprehensive numerical study [38], whilst a comprehensive experimental study

on the structural response of austenitic and duplex stainless steel T-stubs in tension has been conducted by Yuan et al. [39]. Finally, Tao et al [40] recently published a paper on the response of blind-bolted beam-to-concrete filled stainless steel tubular column connections. 4 SHS and 3 CHS concrete filled stainless steel sections were tested under monotonic or cyclic loading with or without the presence of a concrete slab. All tested joints involved a concrete-filled stainless steel column and hence do not lend themselves for the assessment of design provisions for stainless steel joints, as the presence of concrete slab and the interaction of concrete infill and blind bolts complicate the response and affect the developed failure modes.

This brief literature survey highlights the need for full-scale tests on stainless steel beam-to-column joints, given the current worldwide trend towards sustainability, which is expected to favour the more widespread use of stainless steel in construction [41]. In order to complement the currently very limited research on stainless steel joints, this paper reports, for the first time, a systematic experimental and numerical study on stainless steel beam-to-tubular column joints. The experimental and numerical studies reported herein, as well as in [37-39] are an important step towards the assessment of the suitability of current design provisions of EN 1993-1-8 [42], which were originally derived for and are based on the response of carbon steel joints. It is envisaged that certain restrictions of EN 1993-1-4 [43], as for example the fact that plastic global analysis is currently not allowed in the absence of experimental evidence as "there should be evidence that the joints are capable of resisting the increase in internal moments and forces due to strain hardening" can be overcome and novel design provisions in line with the observed response will be developed.

2   Experimental studies

2.1 Specimens

All tested beam-to-tubular column specimens employed a fabricated stainless steel I-section with an outer depth h of 240 mm a flange width b of 120 mm, flange thickness t_f equal to12 mm and web thickness t_w equal to 10 mm (i.e. I 240×120×12×10) for the beam at the end of which the load was applied. Two square hollow sections (SHS) with the same outer dimensions (150×150 mm) but different wall thickness (6mm or 10 mm) were employed as columns. Three connection typologies often employed in steel structures (e.g. steel buildings), have been selected and are studied herein. These are the flush end plate connection (FEP), the top and seat angle cleat connections (TSAC) and the top, seat and double web cleat connection (TSWAC). To minimise cost, the same beam sections were used for the TSAC and TSWAC specimens. To mitigate any adverse effect on the response of the specimens due to reusing the beams, the tests on the TSAC sepcimens which were subjected to overall smaller forces were first conducted. As expected, due to the selected beam size compared to the conneciton details, all plastic deformations were limited in the top and seat angle cleats, the column face and the blind bolts with the beam remaining virually intact and elastic for both TSAC tests. Upon inpsection there was no permanent deformation in the compressed flange of the beam and no ovalisation of the bolt holes of the beam. All fillet welds between the end plates and the I-sections of the FEP specimens had a specified minimum throat thickness of 6 mm and were manufactured using the TIG welding process with ER 308 filler rod.

To induce variations in the obtained structural response and observed failure modes for each joint typology two specimens were tested: one where a thicker (10 mm) SHS was connected to the beam via thinner end plates/angle cleats (specimen 1) and one with a relatively thin-walled (6 mm) SHS was connected to the beam via thicker (10 mm) end plates/angle cleats thus promoting failure of the column face (specimen 2), as shown in Fig. 1 where the geometry of the tested specimens is

reported. All tested joint typologies fall within the semi-rigid range when classifying connections with respect to stiffness. With respect to connection classification according to strength, all of the tested connections were designed to be partial strength so that failure of the connection occurs prior to failure of the connected members. With the exception of specimen TSAC-1, which failed marginally below 25% of the plastic moment resistance of the connected beam (112 kNm) and is hence classified as nominally pinned, all other joints reached higher moments and are hence classified as semi-rigid.

As in the experimental programme reported in [37], M16 in Grade A80 stainless steel bolts have been used in 18 mm clearance holes to connect the angle cleats to the beam section. Since access from one side only was available when bolting the angle cleats or end plates to the column, stainless steel Hollo-bolts were used to facilitate blind-bolted connections. All Hollo-bolts used were M16 in Grade EN 1.4401. In accordance with the specifications by Lindapter [44], 26 mm clearance holes were drilled to accommodate the 25.75 mm outer diameter of the sleeve.

2.2 Material response

The material response of the I-sections used as beams, the angle cleats and the conventional bolts connecting the angle cleats to the beams has been reported in [37]. As part of the experimental programme reported herein, additional material coupons were tested in tension to characterise the material response of the columns, the end plates and the flared sleeves of the Hollo-bolts.

The failure mode of connections involving Hollo-bolts, usually involves pulling out of the Hollo-bolt upon significant bending of the flaring sleeve. Hence the highly nonlinear response and the deformation of the Hollo-bolts is attributable primarily to plastic bending of the sleeve [19]. Being the most important (i.e. experiencing the highest stresses and deformations) part of the Hollo-bolt

connection, the material response of the sleeve requires special consideration. For this reason, a 4 ×3.5 ×41 material coupon was extracted from the sleeve and tested in tension. The sleeve dimensions were such that a strain gauge could be marginally fit within its width, whilst the cross-section was small enough to limit the force the coupon would be subjected to given the limited length over which it was clamped. Coupons were also extracted from the same length of tubes used as columns and from the plates from which the end plates were machined. Both flat and corner coupons were extracted from both SHS (i.e. SHS 150×150×6 and SHS 150×150×10) employed in the joint tests. Since the focus of this study lies in the joint response, flat coupons were extracted only from the column face to which the beam was connected and from an adjacent corner to that face.

Fig.2 depicts a flat coupon during the test and at the formation of necking and a corner coupon at the initiation of the formation of the necking prior to failure. Strain control with an applied strain rate of 0.007%/s up to the 0.2% proof stress $\sigma_{0.2}$ and subsequently a strain rate of 0.025%/s until failure was applied during testing following the provisions of ISO 6892-1 [45]. In Fig.3 the obtained stress-strain curves for the flat and corner coupons of the SHS and for the material of the sleeve of the Hollo-bolts are reported. Similar curves were obtained for all tested material. Key material characteristics as stated in the mill certificates and as obtained from the tensile tests are reported in Tables 1 and 2 respectively, where E is the Young's modulus, $\sigma_{0.2}$, $\sigma_{1.0}$ and σ_u are the 0.2% proof stress, the 1% proof stress and the ultimate tensile stress respectively, ε_f is the strain at fracture and n and m are the strain-hardening exponents of the two-stage Ramberg-Osgood law commonly employed to approximate the material response of stainless steel [46, 47].

Significant discrepancies in the obtained material responses as quantified in terms of the reported proof stress and ultimate tensile stress values can be observed, particularly for the SHS 150×150×10 section, the $\sigma_{0.2}$ of which is seen to be 50% higher in Table 2 compared to the value

reported in the mill certificates. Smaller discrepancies are observed for the ultimate tensile stress. This is attributed to the cold-forming process, which significantly alters the material response and enhances the proof stress and ultimate tensile stress values of cold-formed stainless steel sections, compared to the ones of the virgin material from which the sections were rolled [48]. Additional reasons for the observed discrepancies between values reported in the mill certificates and the ones obtained from this study for proof stresses, ultimate tensile stress and strain at fracture may be attributed to potential differences in material orientation and applied strain rates [49] when the tests were conducted [37], as was previously observed for austenitic stainless steel I-sections [50].

2.3 Setup, instrumentation and load application

Fig. 4 depicts the setup and employed instrumentation used in all tests. The beam and column members used in all tests were 1.5 m long. All conventional bolts were non-preloaded (i.e. snug-tight). Following the manufacturers specifications [44], a 190 Nm tightening torque was applied on the Hollo-bolts using a calibrated torque wrench to plastically deform the sleeve as required and form the connection. The dimensions of the employed beams and columns as well as the applied boundary conditions imposed, ensure that all plastic deformations are limited within the joint region where failure occurs. The columns bottom end was engulfed within a rigid steel sleeve connected to the lab's strong floor that restricted both rotations and translations, whilst the horizontal deformation of the top end of the column was also restricted through its attachment to a reaction frame. The load was applied at the beam end, which was also restrained against twisting.

LVDTs were extensively used to monitor the displacements (or to ensure that there are no displacements – L7 and L10) at key locations of the specimens as shown in Fig. 4, thus allowing the rotations of both the beam and the column in the vicinity of the joint to be determined. Strain gauges were employed to monitor the evolution of strains in critical locations of the connections

with increasing loading. The location and numbering of the strain gauges affixed on the end plates and angle cleats of the tested specimens is shown in Fig. 5. No strain gauges were affixed on the column face of the columns as they would have been damaged by the end plates/angle cleats in contact.

A 400 kN hydraulic actuator with a maximum stroke of 250 mm was used in all tests to apply the load at the beam end, 1.47m from the column face. A constant loading rate of 1.5mm/minute was adopted to obtain the quasi-static response of the joints and eliminate any potential strain rate effects, whilst the loading procedure was halted for at least 2 minutes at regular intervals to visually inspect the specimen and check the recorded results for consistency. A slower loading rate of 1mm/min was applied when significant inelastic deformations developed in the joints, primarily due to concerns relating to a potential sudden bolt pull-out. Clearly in any test on connections the strain rates experienced by various parts of the specimen will vary significantly as different parts of the joint will be subjected to different (or even zero) strains. The adopted loading rate resulted in low strain rates at the extreme fibres of the beam and also in regions of the connection with high stress concentration, as can be deduced from the strain-rotation graphs reported hereafter. It is thus believed that the obtained results are representative of the static response of stainless steel joints. The tests were terminated once significant joint rotations and inelastic deformations occurred in either the column face or the end plates and angle cleats. A joint rotation of 105 mrad, 3 times the minimum rotation value of 35 mrad required by EN 1998-1-1 [51] for dissipative joints in structures characterised as ductility class high (DCH), was deemed high enough for all intents and purposes, whilst it also suffices to characterise the joints' response in terms of both stiffness and strength.

2.4 Results and discussion

The applied moment is determined as the applied force times 1.47, whilst the corresponding joint rotation is defined as the rotation of the beam end Φ_b minus the recorded column shear panel rotation Φ_c, both of which are determined from the LVDT readings. As discussed in [37], the three pairs of LVDTs (i.e. L1 -L2, L3-L4 and L3-L1) that can be used to deduce the beam rotation (i.e. rotation equals the difference of the LVDT readings divided by the distance between the LVDTs), yield identical results in all cases. Table 3 reports a summary of key parameters pertinent to the connection response, which allows the behaviour exhibited by the tested connections to be quantified in terms of rotational stiffness and strength (plastic moment resistance), thus facilitating the discussion and the comparison of the response of the tested joints with design predictions. The key parameters reported in Table 3 include the observed failure modes, the initial rotational stiffness $S_{j,ini}$, the pseudo-plastic moment resistance $M_{j,R}$ and the maximum recorded moment $M_{j,max}$, which is a lower bound for the actual ultimate moment that the joints could attain. Similar to [37], the initial stiffness $S_{j,ini}$ was determined by means of regression analysis of the linear part of the moment-rotation curve, prior to the development of any plastic deformations. Where the initial linear part was preceded by a nonlinear region due to the existence of gaps between the bolts and the clearance holes, the nonlinear region was ignored and the regression analysis was conducted on the linear part of the curve. The pseudo-plastic moment resistance $M_{j,R}$ of each specimen was obtained from the intersection between the initial elastic stiffness and the line tangent to the hardening part of the curve. The ratio of the maximum recorded moment resistance $M_{j,max}$ over the plastic moment resistance $M_{j,R}$ (i.e. overstrength) can be considered another quantifiable measure of ductility and ranges from1.76 for specimen TSAC-2 to 2.45 for specimen TSWAC-1. As previously stated, the recorded maximum moments are not the maximum achievable moments by the tested joints but a conservative lower bound. Nonetheless on average the tested specimens exhibited a recorded maximum moment twice their plastic moment resistance with a coefficient of variation of 0.14. The consistently high overstrength values together with

achieved rotations in excess of 105 mrad indicate the inherent ductility of the tested stainless steel joints. A detailed discussion of the obtained results follows for each joint configuration tested. Since the tests were not conducted to failure, the term failure mode is used herein as synonymous to observed localisation of plastic deformation.

Fig. 6 shows the moment-rotation behaviour recorded from the tests on the specimens with the flush end plate (FEP) configuration. Specimen FEP-1 employs a thicker column section (SHS 150×150×10) and a thinner (6 mm) plate, whilst FEP-2 employs a thicker end plate (10 mm) but a thinner column section (SHS 150×150×6). Both specimens demonstrate a qualitatively similar overall response with a well-defined initially linear moment-rotation behaviour, followed by a rounded curve indicating a progressive loss of stiffness and a second linear branch until the test was terminated at a rotation of 106.4 mrad and 119.2 mrad for the FEP-1 and FEP-2 specimens respectively. By comparing the response of the two specimens, it can be observed that the specimen FEP-1 having a thicker column section displays a better retention of stiffness until approximately half of the maximum recorded load, whilst FEP-2 shows signs of loss of stiffness from about one third of its maximum recorded load.

Figs. 7a and 7b illustrate the observed deformation modes as recorded at the end of the test for both specimens. As intended, two distinct failure modes (i.e. modes of localisation of plastic deformation) were obtained. Significant plastic deformation occurred in the thinner end plate of specimen FEP-1, whilst the much thicker column face remained virtually undeformed. As depicted in Figure 4.7(a), where a close-up of the end plate is also included, plastic bending of the end plate occurred primarily in the vicinity of the top bolt row where higher tensile stresses developed. On the contrary, the thicker (10 mm) end plate of specimen FEP-2 did not show signs of bending and remained undeformed as shown in Fig. 7 (b), where the end plate rotates about the centre of rotation of the connection almost like a rigid body. Limited plastic deformation was also

observed in the vicinity of the bolt holes on the thinner column face. It can thus be deduced in the case of the FEP-2 specimen, plastic deformation was primarily located in the sleeves of the top row of the Hollo-bolts. No signs of plastic deformation were observed in either the compression zone or the shear panel of either joint.

Figs. 8(a) and 8(b) depict the development of strains as rotation is increased for specimens FEP-1 and FEP-2 respectively. The location of the strain-gauges and their numbering have been reported in Fig. 5. In accordance with the sign convention adopted in [37], tensile strains have been assigned a negative sign, whilst compressive strains have been assigned a positive sign. Fig. 8(a) reveals that high plastic tensile strains occur in locations 1, 2, 3 of specimen FEP-1 which were located the farthest from the centre of rotation of the joint and accord well with the deformation mode (i.e. bending) of the plate shown in Fig. 4.7 (a). On the contrary, Fig. 8 (b) shows that only small elastic strains developed in the end plate of specimen FEP-2, as observed in Fig. 7(b).

Fig. 9 depicts the recorded moment-rotation behaviour obtained from the tests on the TSAC-1 and TSAC-2 specimens. A non-linear response with increasing stiffness can be initially observed for both specimens, as the various gaps between the connected parts and the bolts and the bolt holes begin to close and then the initial elastic rotation stiffness is attained. The initially linear elastic response is followed by a gradual loss of stiffness indicated by the rounded part following the first linear branch of the moment-rotation curves. Thereafter a second linear branch follows as the increasing plastic deformations are accompanied by strain hardening of the plastically deformed regions of the joint. TSAC-1, which employs thinner angle cleats (8 mm) exhibits a hardening response following the second linear branch attributable to the progressive flattening of the thin top angle cleat, whereupon forces are transferred by tension rather than bending, hence the joint exhibiting a stiffer response.

In Fig. 10 the deformed shape of specimens TSAC-1 and TSAC-2 is shown. High plastic deformations can be observed in the tension zone of both specimens, whilst in the compression zone of both specimens, the seat cleats are bent. However, the source of the plastic deformation is different in each specimen. It can be clearly seen that specimen TSAC-1, having a thicker column face than angle cleat, exhibited localisation of plastic deformation exclusively in the top angle cleat which bent significantly. Neither, the bolts connecting the top angle cleat to the column face, nor the column face itself show any evidence of plastic deformation and there is no separation between the top cleat and the column face near the connecting bolts. In the case of specimen TSAC-2, which employs thicker (10mm) angle cleats and a thinner column face (6 mm), plastic deformations occur not only at the top angle cleat, but also extend to the column face and the sleeve of the Hollo-bolt, as can be seen in Fig. 10(b). This is due to the thicker and hence stiffer angle cleats attracting higher tensile stresses in the tension zone which lead to plastic deformation of the column face and Hollo-bolt sleeve and partial pull-out of the Hollo-bolt. The low tensile stresses developing in the tension zone of specimen TSAC-1do not suffice to cause pull-out of the Hollo-bolt. Both the Hollo-bolts and the column face are sufficiently stronger than the angle cleat to ensure that the vertical leg of the top cleat remains connected to the column face whilst it undergoes significant plastic bending, which allows further rotation of the joint.

In Figs. 11(a) and 11(b) the development of strains in the top angle cleats connecting the tension flange of the beam to the flange of the column with increasing joint rotation is reported for specimens TSAC-1 and TSAC-2 respectively. The same sign convention as before is adopted. The evolution of strains is distinctly different for specimens TSAC-1 and TSAC-2, as the deformation modes of the angle cleats in each of the specimens are different. For both specimens, high tensile strains on either side of the corner of the angle cleat (locations 2 and 3) can be observed, due to plastic bending (i.e. flattening) of the angle cleats. However, in the case of TSAC-1 the strains increase until the end of the test, whilst for specimen TSAC-2 the increase of

strain in locations 2 and 3 stops at a rotation of about 60 mrad, indicating that at this rotation plastic deformations localized primarily in the bolt hole region of the column face and the bolts. A marked difference in the evolution of strains in location 4 can be observed. Since the vertical leg of the top angle cleat of TSAC-1 bents plastically, location 4 being on the concave side of the bent angle cleat experiences high inelastic compressive strains, whilst very small strains are recorded in the same location for specimen TSAC-2. Finally, very small deformations and strains are seen to develop between the bolt holes on the horizontal leg of the top angle cleat (location 1).

In Fig. 12 the moment-rotation behaviour obtained from the tests on specimens TSWAC-1 and TSWAC-2 is reported. Due to the web cleats connecting the beam to the column via to additional bolt rows, the TSWAC specimens are seen to demonstrate superior rotational stiffness and strength compared to their TSAC counterparts, as expected. Both specimens display similar overall response with the specimen employing the thicker column (TSWAC-1) having slightly higher stiffness but increasingly higher strength than TSWAC-2, as the second linear branch of the curves diverge. Figs 13(a) and 13(b) show the deformed configurations at the end of the tests for TSWAC-1 and TSWAC-2 respectively. In the case of TSWAC-1, due to the column face being significantly stronger and stiffer than the angle cleats, plastic deformation seems to be exclusively occurring in the top and web cleat with some bending of the seat cleat, with the remaining specimen remaining undeformed. In specimen TSWAC-2 plastic deformations occur in the cleats, the column face and the Hollo-bolts, indicating that the joint response is the combined effect of all those components.

In Figs. 14(a) and 14(b) the development of strains in the web cleats of the tension zone of the joint (top and web cleat) is depicted for TSWAC-1 and TSWAC-2 respectively. For both specimens, high tensile strains occur in locations 2, 3 due to bending of the top cleat with increasing rotations, whilst the strains in locations 1 and 5 are insignificant. Tensile strains are also recorded in the vicinity of the corner of the web cleat (locations 6 and 7), with specimen TSWAC-

1 exhibiting higher strains than specimen TSWAC-2 in location 6, since the web cleat of TSWAC-1 deforms significantly more. As in the case of the TSAC specimens, a marked difference can be observed in the evolution of strains in location 4 for both specimens, with specimen TSWAC-1 experiencing high compressive strains due to bending of the vertical leg of the top cleat, whilst the strain in location 4 in specimen TSWAC-2 is very small. A similar trend is observed for the evolution of strains in location 8.

3   Numerical studies

3.1 Development of FE model

In parallel with the experimental studies, nonlinear three dimensional finite element models were developed using the general purpose FE software ABAQUS and validated against the previously reported experimental tests. To this end, the measured geometry and material properties reported previously have been utilised, whilst the employed support conditions reflected the ones used in the tests. All joint components were discretised with the eight-noded (hexahedron) 3D solid element C3D8R with reduced integration, except for the welds between the end plate and the beam, which were simulated using tie constraints. A finer mesh density was employed in areas of high stress gradients (i.e. angle cleats, near the bolt holes etc), whilst 3 elements were used through the thickness of each component as discussed in [38]. Following past studies on the response of stainless steel members [52], the material properties of corner regions were assumed to extend up to 2 times the thickness into the flat region of the tubular column faces; hence the corner regions and their vicinity were assigned the corner material properties, whilst the flat parts of the tubular columns were assigned the flat material properties reported in Table 2. In accordance with [38], the measured material properties reported in Table 2 were used to define the parameters of a 2-stage Ramberg-Osgood approximation [46,47] of the recorded stress-strain

response, using the traditional Ramberg-Osgood curve up to $\sigma_{0.2}$ and a similar curve thereafter up to σ_u [47]. Contact was assumed as hard in the normal direction, whilst the penalty method with a friction coefficient equal to 0.3 was used to simulate contact in the tangential direction, in accordance with the modelling assumptions reported in [38].

To reduce computational time, the threaded geometry of the bolt shank of standard bolts was simulated as a smooth cylinder with a cross-sectional area equal to the stress area of the real bolts, whilst similar assumptions were made for the bolt heads and nuts, which were modelled as cylindrical. Given the complex geometry of the Hollo-bolt and the various interacting part it comprises, a pragmatic approach was followed, and the geometry of the various parts was simplified without compromising accuracy. The bolt shank was assumed to be prismatic, whilst a smooth geometry was assumed for the sleeve and the cone as well. The geometric idealisation of the various components of the Hollo-bolt is shown in Fig. 15. Small sliding contact formulation was assumed at the interface between the sleeve and the cone and the sleeve and the bolt shank, since no sliding is expected or has been observed between the various parts of the Hollo-bolt. The external surface of the bolt and the internal surface of the cone were tied together via a tie constrain to simulate the clamping effect that the presence of the threads would have had and prevent any relative deformation between the cone and the shank on which it is screwed.

For simplicity, the application of the tightening torque and the plastic deformation of the sleeve from its initial undeformed to its final configuration was not explicitly modelled. Instead the final geometric configuration that the bolt sleeve assumes once the required preload value is applied has been simulated and the flaring of the sleeve was assumed to match the angle of the cone in accordance with similar studies [19-21]. Not accounting for the actual deformation of the sleeve may lead to inaccuracies due to deviations of the actual geometry of the sleeve from the idealised one and the deformation history of the sleeve affecting its material properties. Wang et al. [19] conducted a sensitivity study on the effect of the actual geometry of the flaring sleeve and

determined that the effect of a variation of the flaring angle of the sleeves by as much as 20^0 from the nominal angle of 15^0 does not lead to any appreciable difference in either stiffness or strength of the bolt, whilst past studies [19-21] have indicated that satisfactory replication of experimental data can be achieved without due account of the actual stress state of the sleeve at the beginning of the simulation. Contrary to the standard bolts, which were hand-tightened, the Hollo-bolts were preloaded with a torque of 190 Nm to deform the sleeve in the desired geometric configuration and enable the blind-bolted connection to be formed according to the manufacturers guidelines. Hence, although the geometry of the sleeve was modelled in its final configuration, application of the preload on the bolt shank has been explicitly simulated as bolt preload has been shown to significantly affect the obtained stiffness of bolted joints [39]. To incorporate the effect of preloading in the analysis, the analysis was divided into three sequential steps, for each of which a nonlinear static analysis was performed:

1. All Hollo-bolts were pre-tensioned by using the bolt load functionality of ABAQUS

2. The length of the Hollo-bolts was fixed at the end of the first step by using "bolt length control" option.

3. A point load was applied at the end of the beam.

3.2 Model validation

The accuracy of the numerical models is quantified and assessed in terms of the initial rotational stiffness $S_{j,ini}$, the plastic moment resistance $M_{j,R}$ and the maximum recorded moment at the rotation at which the tests were terminated $M_{j,max}$. Table 4 provides where the ratio of the numerical predictions over the respective experimental values. Except for specimen FEP-2, the initial rotational stiffness of which was poorly predicted, a very close agreement between the experimental and the numerically determined initial rotational stiffness is observed. The reported high coefficient of variation of 0.28 reduces to 0.07 if joint FEP- 2 is not considered. The drastic

improvement of the FE predictions for the tubular column joints in terms of the initial rotational stiffness compared to the respective models for the beam-to-open column joints [38] is believed to be related to the applied preload of the Hollo-bolts, which effectively removed any gaps between the various connected parts. Bolt preloading eliminates any gaps between the connected parts thus allowing all components of the connection to be effective from the onset of loading and reducing the effect of fabrication tolerances on the initial rotational stiffness and making the joint rotational stiffness easier to predict.

In terms of plastic moment resistance, the FE models are seen to consistently underestimate the experimental plastic moment resistance by approximately 8%. This is deemed accurate enough to proceed to parametric studies, given the differences of the procedure by which the experimental and numerical $M_{j,R}$ is determined [37, 53]. Finally, the moment at the maximum applied rotation is reasonably well predicted. A detailed comparison between the experimental and numerical results in terms of obtained failure modes and overall moment-rotation response is given in Figs. 16 and 17 respectively where a very close agreement between the two can be observed. It is noted that, as observed in Fig. 17 (b), the numerical curve does not accurately capture the initial response of specimen FEP- 2 and significantly underpredicts its stiffness, but the agreement between the two curves drastically improves with increasing rotations and the two curves practically coincide beyond a rotation of 20 mrad. The higher rotational stiffness exhibited by the test specimen may be attributed either to experimental errors or to a higher preload accidentally applied to some of the Hollo-bolts.

3.3 Parametric studies

Upon validation of the FE models, parametric studies were performed to enable the study of the behaviour of austenitic stainless steel connections over a wide range of geometric configurations and highlight the influence of key joint details on the overall response. The beam-to-tubular

column joint typologies against which the FE models were calibrated, namely FEP, TSAC and TSWAC are employed in the parametric studies. In all cases the experimentally determined material response was adopted for the bolts and the connected members. The investigated parameters include the thickness of the end plate/angle cleats t_p/t_a, the thickness of the tubular column t_c, the bolt edge distance e_2 between the centre of the bolt hole and the edge of the plate, the distance between the bottom beam flange and the top bolt row z and the length of the angle cleat leg L_1 with the bolt hole located in all cases 35 mm below the tip of the angle cleat. A total of 54 parametric analyses were performed. For all cases considered, failure was triggered by bolt or by Hollo-bolt legs failure and pull out of bolt clearance holes, since the bolts possess markedly reduced ductility compared to the other joint components as indicated by their significantly lower plastic strain at fracture ε_f. The obtained results are discussed in the following section.

4   Results and discussion

4.1 Effect of key parameters on joint response

Fig. 18 shows the effect of each of the investigated parameters on the structural response in terms of the obtained moment rotation curve. As expected, increasing the lever arm z, or the edge distance e_2, leads to a marked increase of both the strength and the stiffness of the connections. Increasing the end plate thickness t_p also increases the strength and the stiffness of the joints by increasing the resistance of the equivalent T-stub [42]. However, the effect is less pronounced as increasing the end plate thickness beyond a certain value (beyond 12 mm for the parameter range considered herein), shifts the failure mode to the column flange, which becomes the weakest component of the connection. Similarly, increasing the column flange thickness t_f beyond 12 mm has a limited effect on the strength and stiffness as the end plate is already the weakest component of the joint, whilst decreasing it more drastically affects the joint response, by shifting the failure mode from the end plate to the column flange. In all cases, an increase in strength is accompanied by a corresponding decrease in the rotation at which the ultimate moment occurs.

Despite the top angle cleat being arguably the critical component affecting the response, both top and bottom cleats were assumed identical in all parametric studies. In Figs. 18(a) and (b) it can be observed that increasing the angle thickness or decreasing the length of its leg significantly enhances both the strength and the stiffness of the TSAC joints, but leads to a drop in the rotation at ultimate moment $\Phi_{j,u}$, since the thicker (or shorter) and hence stiffer angles transfer a higher tensile force and cause bolt failure at smaller deformations compared to the thin ones. The effect of flattening due to large inelastic bending of the top cleat is shown in the bottom two curves of Figs. 19(a) and (b), where an increase of the joint stiffness can be observed at large rotations, arguably due to the angle cleat transmitting forces primarily in tension instead of bending.

On the other hand, the effect of bolt edge distance e_2 is negligible since, contrary to the end plate connections, the edge distance does not affect the effective leg of the equivalent T-stub, which is in agreement with the design provisions of EN 1993-1-8 [42]. Changing the column face thickness t_c only has an effect when the column face becomes weaker than the angle cleat and hence the failure mode is shifted from the cleat to the column face, thus resulting in different response, as can be seen in Fig. 19 (c), where except for the lower curve, all other curves are identical. Similar observations can be made for TSWAC joints, as can be seen in Fig. 20.

4.2 Assessment of design predictions for blind-bolted joints

In all subsequent calculations the measured geometric and material properties are used for the joint components and all safety factors were set to unity. For specimens FEP-1 and TSAC-1 the behaviour of which is governed by bending of the end plates and angle cleats respectively, the design provisions codified in EN 1993-1-8 [42] are used to predict the joint moment resistance, whilst for specimen TSWAC-1 the recommendations by Pucinotti [54], which extend the scope of application of the EN 1993-1-8 [42] are used in accordance with previous studies [37, 38]. For specimens the response of which involves plastic bending of the column face, Eq. (1) has been

employed for the determination of the plastic resistance of the column face component, which is specified in SCI/BCSA [26].

$$F_{y,SCI} = \frac{2\sigma_y t_c^2}{1-\beta_1}\left[\frac{(n_r-1)p - 0.5 n_r d_{bh}}{b_0 - 3t_c} + 1.5(1-\beta_1)^{0.5}(1-\gamma_1)^{0.5}\right] \tag{1}$$

where σ_y is the material yield stress, p is the bolt pitch distance, $\beta_1 = g/(b_o - 3t_c)$ and $\gamma_1 = d_{bh}/(b_o - 3t_c)$, g being the gauge width (i.e. horizontal distance) between the bolts, b_o the outer width of the tubular column face to which the connection is made, t_c the thickness of the face of the tubular columns and d_{bh} the diameter of the clearance hole of the Hollo-bolts.

The stiffness of the column face component in bending k_{cf} is determined according to Eq. 2, which was proposed by Málaga-Chuquitaype and Elghazouli [22] for the stiffness of the face of carbon steel SHS sections in bending.

$$k_{cf} = \frac{\pi \cdot E \cdot t_c^3}{12(1-\nu^2)\cdot 0.18(\frac{b_c - t_c}{2})^2} \tag{2}$$

,where E and ν are the Young's modulus and Poisson's ratio of the material of the column face, and b_c and t_c are the outer width and thickness of the column face respectively.

For the determination of the stiffness of the Hollo-bolts in tension the predictive model proposed by Wang et al. [19] for Hollo-bolts has been used. The proposed model accounts both for the axial elongation of the bolt shaft in tension according to the codified provisions and for the deformation of the flaring sleeves. Upon determination of the stiffness of all relevant components, Eq. 3 is utilized to determine the initial rotational stiffness of the joints, where all symbols have been previously defined.

$$S_{j.ini} = \frac{Ez^2}{\sum_i \frac{1}{k_i}} \tag{3}$$

where E is Young's modulus, z is the lever arm of the joint and k_i is the component stiffness of each relevant component as defined in [42].

In Table 5 the predicted analytical values for stiffness and strength of the tested joints are compared against the experimental ones. On average the stiffness predictions overestimate the experimentally determined stiffness by 35% with a coefficient of variation of 0.50, thus indicating the inaccuracy of the stiffness predictions. Similar conclusions were reported [36] and [37]. In terms of the pseudo-plastic moment resistance predictions $M_{j,R}$ of the joints, in all cases the design predictions yield overly conservative results. The predicted-to-experimental ratio for the moment resistance is on average 0.50 with a coefficient of variation 0.18. A similar level of conservatism of the EN 1993-1-8 [42] design predictions was reported for stainless steel T-stubs in tension by [39] and for stainless steel beam-to-column joints reported [37], where the predicted-over-experimental resistance was 0.51 and 0.53 respectively with a coefficient of variation of 0.13 in both cases.

Similar conclusions can be drawn when the 54 FE results are used to assess the stiffness and strength predictions for stainless steel beam-to-tubular column joints, as shown in Table 6. The stiffness is well predicted for the FEP joints, whilst it is over-predicted for the TSAC and TSWAC joints. In terms of the plastic moment resistance, the predictive models yield significantly and consistently conservative results with a mean ratio of the predicted over the numerical moment resistance ranging from 0.42 to 0.66 and a small coefficient of variation (0.09 to 0.13). Similar conclusions were drawn in [36, 38], where the stiffness predictions were generally scattered, whilst the strength predictions were consistently conservative. The conservative moment capacity predictions for stainless steel joints are due to the fact that predictive models limit the maximum attainable stress value to the nominal 0.2% proof stress $\sigma_{0.2}$. Joints generally experience high deformations and strains when their response is governed by a ductile failure mode such as

bending of the end plate, angle cleat or column flange, hence the pronounced strain-hardening of stainless steel leads to significantly higher attainable stresses. Possible remedies of this shortcoming include the adoption of a material model incorporating the effect of strain-hardening when determining the design resistance of each connection component and allowing stresses in excess of the nominal yield stress to be attained provided the corresponding failure mode is ductile.

5   Conclusions

Owing to the lack of available experimental data on stainless steel connections, current design rules [42] are based on assumed analogies with carbon steel design, thereby neglecting the high ductility and pronounced strain-hardening exhibited by stainless steels. This paper addresses this gap in knowledge and reports a systematic experimental and numerical study on stainless steel beam-to-tubular column joints that allows for a better understanding of their behaviour and the assessment of current design approaches for both strength and stiffness. Six full-scale beam-to-tubular column connections in austenitic stainless steel have been reported in detail. The tested specimens were designed such that different failure modes developed, thus allowing a wide range of structural responses to be experimentally studied. In all cases the joints exhibited significant inelastic deformations with recorded rotations more than 105 mrad, far beyond the limit of 35 mrad required for dissipative joints in structures classified as DCH (ductility class high). The achieved rotations are deemed sufficient to obtain both the initial rotational stiffness and the joint moment resistance $M_{j,R}$, whilst the rotation capacity recorded is clearly a lower bound of the available rotation capacity of the joint.

In parallel, advanced FE models able to accurately simulate the overall moment-rotation response and failure modes of stainless steel beam-to-tubular column joints were developed and validated against the reported experimental data. The validated models were used to generate 54 numerical

data on stainless steel joints. Based on both experimental and numerical results, design predictions for stiffness and plastic moment resistance were assessed. In all cases the predicted joint moment resistance was significantly underestimated, whilst the stiffness predictions were inaccurate. Similar conclusions were drawn in [36-39] for stainless steel beam-to-open section column joints. It is thus concluded that the development of more efficient design guidance for stainless steel beam-to-tubular column joints, which allows for the explicit incorporation of strain hardening in the design procedure in line with the observed structural response, is warranted.

Acknowledgements

References

[1] Ogden R.G., Baddoo N.R., Burgan R. (1997) Architects' guide to stainless steel P179. The Steel Construction Institute.

[2] T.M. Chan, L. Gardner. (2008). Compressive resistance of hot-rolled elliptical hollow sections. Engineering Structures, 30(2): 522-532.

[3] Theofanous M., T.M. Chan, L. Gardner. (2009). Structural response of stainless steel oval hollow section compression members. Engineering Structures 31(4): 922-934.

[4] Pitrakkos T., Tizani W. (2013). Experimental behaviour of a novel anchored blind-bolt in tension. Engineering Structures 49:905-919.

[5] Tizani W., Pitrakkos T. (2015). Performance of T-Stub to CFT Joints Using Blind Bolts with Headed Anchors. Journal of Structural Engineering 141(10): 04015001.

[6] White R.N., Fang , P.J. (1966). Framing connections for square structural tubing. Journal of the Structural Division, American Society of Civil Engineering 92: 175–194.

[7] Dawe J.L., Grondin G.Y. (1990). W-shape beam to RHS column connections.Canadian Journal of Civil Engineering, 17: (5): 788-797.

[8] Sherman D., Ales J.M. (1991). The design of shear tabs with tubular columns. AISC Proc. National Steel Construction Conference.

[9] Maquoi R., Naveau X., Rondal J. (1984) Column welded stud connections. Journal of Constructional Steel Research 4: 3–26.

[10] Korol, R.M., Ghobarah, A. and Mourad, S. (1993) Blind bolting W-shape beams to hss columns. Journal of Structural Engineering-ASCE 119(12): 3463-3481.

[11] Málaga Chuquitaype C., Elghazouli A.Y. (2010). Behaviour of combined channel/angle connections to tubular columns under monotonic and cyclic loading. Engineering Structures 32(6): 1600-1616.

[12] Schneider S.P., Alostaz Y.M. (1998). Experimental Behavior of Connections to Concrete-filled Steel Tubes. Journal of Constructional Steel Research 45(3): 321-352.

[13] Han L.H., Wang W.D., Zhao X.L. (2008). Behaviour of steel beam to concrete-filled SHS column frames: Finite element model and verifications. Engineering Structures 30(6): 1647-1658.

[14] Hoang V.L., Demonceau J.F., Jaspart J.P. (2014). Resistance of through-plate component in beam-to-column joints with circular hollow columns. Journal of Constructional Steel Research 92: 79–89.

[15] J. Yang, T. Sheehan, X.H. Dai, D. Lam. (2015). Experimental study of beam to concrete-filled elliptical steel tubular column connections. Thin-Walled Structures 95: 16-23.

[16] Azizinamini A., Shekar Y., Saadeghvaziri M.A. (1995). Design of through beam connection detail for circular composite columns. Engineering Structures 17(3): 209-213.

[17] Hoang V-L, Jaspart J-P, Demonceau J-F. Extended end-plate to concrete-filled rectangular column joint using long bolts. J Constr Steel Res 2015; 113: 156-168.

[18] Elghazouli AY, Málaga-Chuquitaype C, Castro JM, Orton AH. (2009). Experimental monotonic and cyclic behaviour of blind-bolted angle connections. Engineering Structures 41: 2540-2553.

[19] Wang, Z., Tizani, W., Wang, Q. (2010) Strength and initial stiffness of a blind-bolt connection based on the T-stub model. Engineering structures 32: (9): 2505-2517.

[20] Liu, Y., Malaga-Chuquitaype, C. and Elghazouli, A.Y. (2012). Behaviour of beam to-tubular column angle connections under shear loads. Engineering structures 42: 434-456.

[21] Liu, Y., Malaga-Chuquitaype, C. and Elghazouli, A.Y. (2012). Response and component characterisation of semi-rigid connections to tubular columns under axial loads. Engineering structures 41: 510-532.

[22] Málaga-Chuquitaype, C. and Elghazouli, A. (2010). Component-based mechanical models for blind-bolted angle connections. Engineering structures, 32: (10): 3048-3067.

[23] Wang, Z.-Y. and Wang, Q.-Y. (2016) Yield and ultimate strengths determination of a blind bolted endplate connection to square hollow section column. Engineering structures, 111: 345-369.

[24] Kurobane Y., Packer J.A., Wardenier J., Yeomans N. (2004). Design guide for structural hollow section column connections. CIDECT. The International Committee for Research and Technical Support for Hollow Section Structures.

[25] Gomes, F., Jaspart, J.-P. and Maquoi, R. (1996) Moment capacity of beam-to-column minor-axis joints Proceedings of the IABSE Colloquium on Semi-Rigid Structural Connections., 319-326.

[26] SCI/BCSA (2005) British Constructional Steelwork Association Joints in Steel Construction: Moment Connections. Steel Construction Institute and the British Constructional Steelwork Association (P207).

[27] Pitrakkos T., Tizani W. (2015). A component method model for blind-bolts with headed anchors in tension. Steel and Composite Structures 18(5): 1305-1330.

[28] Mahmood, M., Tizani, W., Sansour, C. (2015). Effect of Bolt Gauge Distance on the Behaviour of Anchored Blind Bolted Connection to Concrete Filled Tubular Structures. In: Proceedings of the 15th International Symposium on Tubular Structures, pp. 87-93.

[29] Cai Y., Young, B. (2014). Structural behaviour of cold-formed stainless steel bolted connections, Thin-Walled Structures 83: 147-156, 2014.

[30] Cai Y., Young, B. (2014). Behaviour of cold-formed stainless steel single shear bolted connections at elevated temperatures, Thin-Walled Structures 75: 63-75, 2014.

[31] Cai and Young (2015). High temperature tests of cold-formed stainless steel double shear bolted connections. Journal of Constructional Steel Research, 104: 49-63.

[32] Feng R., Young B. (2008) Experimental investigation of cold-formed stainless

steel tubular T-joints. Thin-Walled Structures, 46: (10): 1129-1142.

[33] Feng R., Young B. (2008) Tests of concrete-filled stainless steel tubular T-joints.

Journal of Constructional Steel Research, 64: (11): 1283-1293.

[34] Feng R., Young B. (2010) Tests and behaviour of cold-formed stainless steel

tubular X-joints. Thin-Walled Structures, 48: (12): 921-934.

[35] Feng R., Young B. (2013) Stress concentration factors of cold-formed stainless

steel tubular X-joints. Journal of Constructional Steel Research, 91: 26-41.

[36] Hasan M.J., Ashraf M., Uy B. (2017) Moment-rotation behaviour of top seat angle bolted connections produced from austenitic stainless steel. Journal of Constructional Steel Research 136: 149-161.

[37] Elflah M., Theofanous M., Dirar S., Yuan H. (2019). Behaviour of stainless steel beam-to-column joints—Part 1: Experimental investigation. Journal of Constructional Steel Research 152: 183-193.

[38] Elflah M., Theofanous M., Dirar S. (2019). Behaviour of stainless steel beam-to-column joints—Part 2: Numerical modelling parametric study. Journal of Constructional Steel Research 152: 194-212.

[39] Yuan H.X., Hu S., Du X.X., Yang L., Cheng X.Y., Theofanous M. (2019). Experimental behaviour of stainless steel bolted T-stub connections under monotonic loading. Journal of Constructional Steel Research 152: 213-224.

[40] Tao Z., Hassan M.K., Song T.-Y., et al. (2017) Experimental study on blind bolted connections to concrete-filled stainless steel columns. Journal of Constructional Steel Research, 128: 825-838.

[41] Rossi B. (2014) Discussion on the use of stainless steel in constructions in view of sustainability. Thin-Walled Structures, 83: 182-189.

[42] EN 1993-1-8. (2005). Eurocode 3: Design of steel structures – Part 1.8: Design of joints. British Standards Institution, CEN.

[43] EN 1993-1-4+A1. (2015). Eurocode 3: Design of steel structures–Part 1.4: General rules–supplementary rules for stainless steel, CEN.

[44] Lindapter International. (2018). Type HB Hollo-bolt for blind connection to structural steel and structural tubes.

[45] BS ISO 6892-1 (2009) Metallic materials. Tensile testing. Method of test at ambient temperature. BSI.

[46] Mirambell E., Real E. (2000). On the calculation of deflections in structural stainless steel beams: an experimental and numerical investigation. Journal of Constructional Steel Research 54: (1): 109-133.

[47] Rasmussen K.J.R. (2003). Full-range stress–strain curves for stainless steel alloys. Journal of Constructional Steel Research, 59: (1): 47-61.

[48] Afshan S., Rossi B., Gardner, L. (2013) Strength enhancements in cold-formed structural sections—Part I: Material testing. Journal of Constructional Steel Research, 83: 177-188.

[49] Huang Y., Young B. (2014). The art of coupon testing. Journal of Constructional Steel Research 96: 159–175

[50] Gardner L., Bu Y., Theofanous M. (2016). Laser-welded stainless steel I-sections: Residual stress measurements and column buckling tests. Engineering Structures 127: 536-548.

[51] EN 1998-1 (2004). Eurocode 8: Design of structures for earthquake resistance - Part 1: General rules, seismic actions and rules for buildings. . British Standards Institution, CEN.

[52] Gardner L., Nethercot D.A.(2004). Numerical modeling of stainless steel structural components - a consistent approach. Journal of Structural Engineering 130(10): 1586-1601.

[53] Girão Coelho A.M., Bijlaard F.S.K. (2007). Experimental behaviour of high strength steel end-plate connections. Journal of Constructional Steel Research, 63(9): 1228-1240.

[54] Pucinotti R. (2001). Top-and-seat and web angle connections: prediction via mechanical model

Journal of Constructional Steel Research 57(6): 663-696.

Table 1: Material properties according to mill certificates

Specimen	$\sigma_{0.2}$	$\sigma_{1.0}$	σ_u	ε_f
	(N/mm^2)	(N/mm^2)	(N/mm^2)	%
I-240×120×12×10	341	369	635	53
L-100X100X8	373	441	675	54
L-100X100X10	378	445	673	55
Endplate (6 mm)	387	419	644	50
Endplate (10 mm)	334	376	620	53
SHS 150×150×6	284	338	612	56
SHS 150×150×10	336	377	617	53

Table 2: Key material properties from tensile coupon tests

Specimen	E	$\sigma_{0.2}$	$\sigma_{1.0}$	σ_u	ε_f	n	m
	(N/mm^2)	(N/mm^2)	(N/mm^2)	$(N/mm^2$	%		
I-240×120×12×10 - flange	196 500	248	306	630	66	5.20	2.37
I-240×120×12×10 - web	205 700	263	320	651	65	6.70	2.41
Angle cleat (8 mm)	197 600	280	344	654	55	12.22	2.49
Angle cleat (10 mm)	192 800	289	354	656	56	10.62	2.54
End plate (6 mm)	201 000	289	357	658	62	12.20	2.53
End plate (10 mm)	195 000	276	339	636	51	11.05	2.51
SHS 150×150×6 - flat	189 650	334	373	640	63	8.03	2.80
SHS 150×150×6 - corner	210 420	647	703	795	46	11.00	3.83
SHS 150×150×10 - flat	200 020	507	540	730	51	8.40	3.43
SHS 150×150×10 - corner	198 000	608	692	796	47	4.93	3.67
Sleeve of blind bolt (4 mm)	180 000	381	533	735	32	17.24	3.68

Table 3: Key test results

Specimen	Initial stiffness $S_{j,ini}$ (kNm/rad)	Maximum moment $M_{j,max}$ (kNm)	Plastic Moment resistance $M_{j,R}$ (kNm)	maximum recorded rotation Φ_c (mrad)	Observed deformation mode at the end of the test
FEP-1	2100	46.9	27	106.4	End plate in bending / Mode 1
FEP-2	1845	28.8	17	119.2	Deformation/partial pull-out of Hollo-bolts
TSAC-1	712	26.0	12	126.5	Bending of flange cleat/Mode1
TSAC-2	770	31.5	18	108.5	Bending of column face/partial pull-out of Hollo-bolts
TSWAC-1	1421	56.7	21	114.4	Bending of flange/Mode 1- bending of web cleat /Mode 1
TSWAC-2	1112	49.7	28	120.9	Bending of column face/partial pull-out-of Hollo-bolts

Table 4: Comparison of FE results with test results

Specimen	FE/Test ratio		
	Initial stiffness $S_{j,ini}$	Plastic Moment resistance $M_{j,R}$	Maximum moment $M_{j,max}$
FEP- 1	1.06	0.93	1.09
FEP- 2	0.40	0.88	1.03
TSAC- 1	0.92	0.92	1.08
TSAC- 2	0.98	0.94	0.93
TSWAC- 1	0.98	0.95	1.07
TSWAC- 2	1.11	0.89	0.98
MEAN	0.91	0.92	1.03
COV	0.28	0.03	0.06

Table 5: Assessment of predictive models based on test results

Specimen	Initial stiffness $S_{j,ini}$ (kNm/mrad)			Moment Capacity M_j (kNm)		
	$S_{j,ini,}$ (predicted)	$S_{j,ini}$ (TEST)	Predicted/Test ratio	$M_{j,R}$ (predicted)	$M_{j,R}$ (TEST)	Predicted/Test ratio
FEP-1	2241	2100	1.06	10.0	27	0.37
FEP-2	776	1845	0.42	7.4	17	0.44
TSAC-1	1500	712	2.10	6.6	12	0.55
TSAC-2	818	770	1.06	9.2	18	0.51

TSWAC-1	3161	1421	2.22	13.2	21	0.63	
TSWAC-2	1376	1112	1.23	14.9	28	0.53	
MEAN			1.35			0.50	
COV			0.50			0.18	

Table 6: Assessment of predictive models based on FE results

Joint type	Predicted/Test stiffness $S_{j,ini}$		Predicted/Test moment capacity $M_{j,R}$	
	MEAN	Coefficient of variation	MEAN	Coefficient of variation
FEP (20 data points)	1.07	0.17	0.42	0.09
TSAC (17 data points)	2.08	0.21	0.65	0.09
TSWAC (17 data points)	2.05	0.19	0.66	0.13
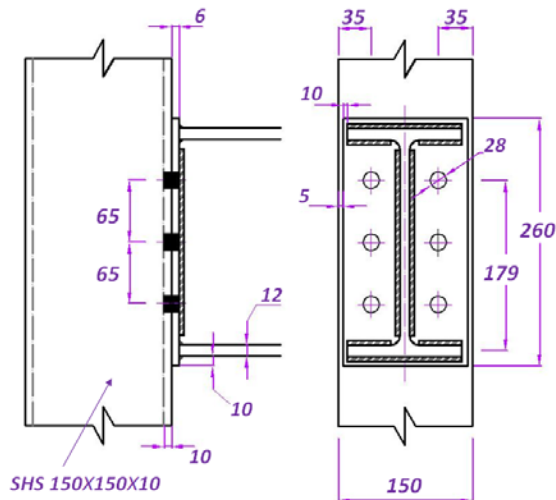
(a) Flush End Plate (FEP-1) connection
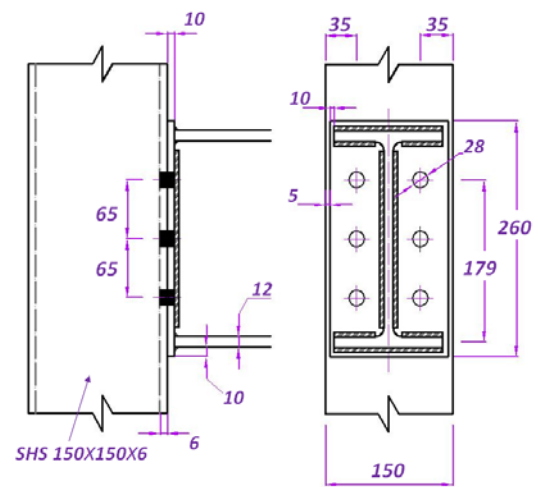
(b) Flush End Plate (FEP-2) connection
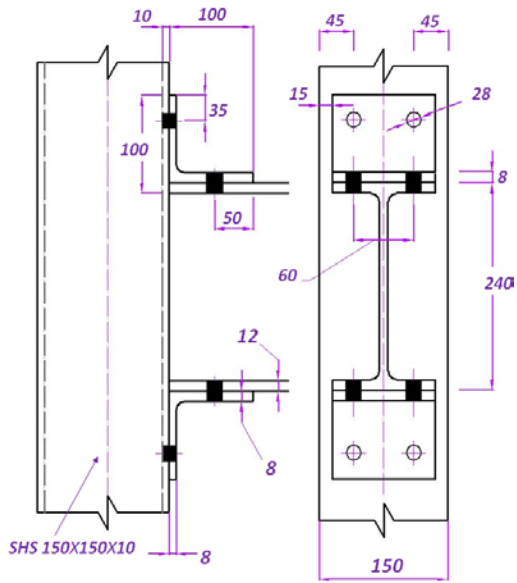
(c) Top and Seat Angle Cleat connection (TSAC-1)
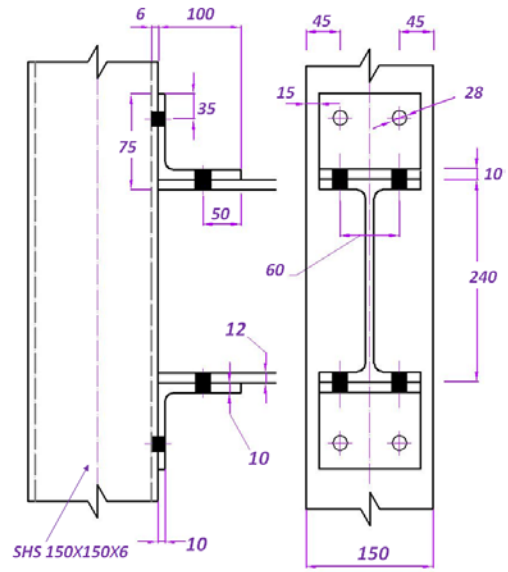
(d) Top and Seat Angle Cleat connection (TSAC-2)
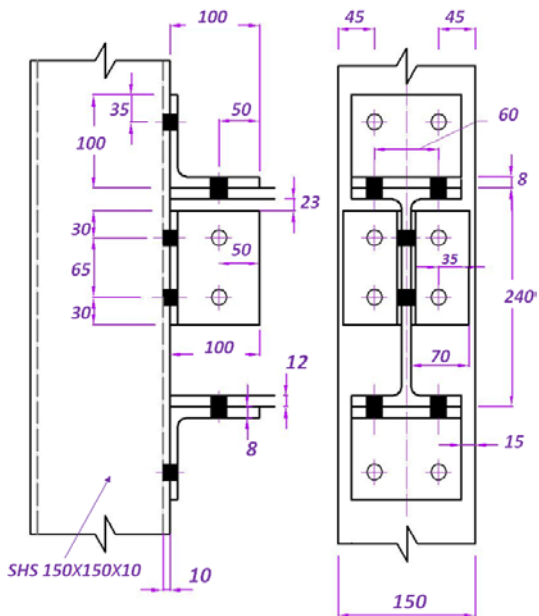
(e) Top, Seat and double Web Cleat connection (TSWAC-1)
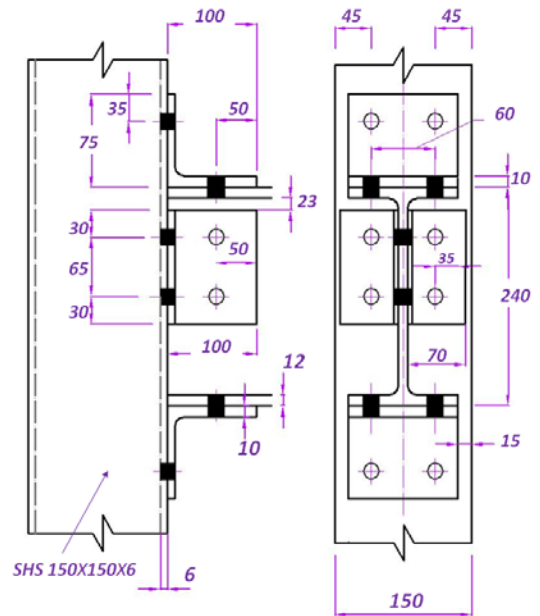
(f) Top, Seat and double Web Cleat connection (TSWAC-2)

Fig. 1: Geometry of the tested specimens.
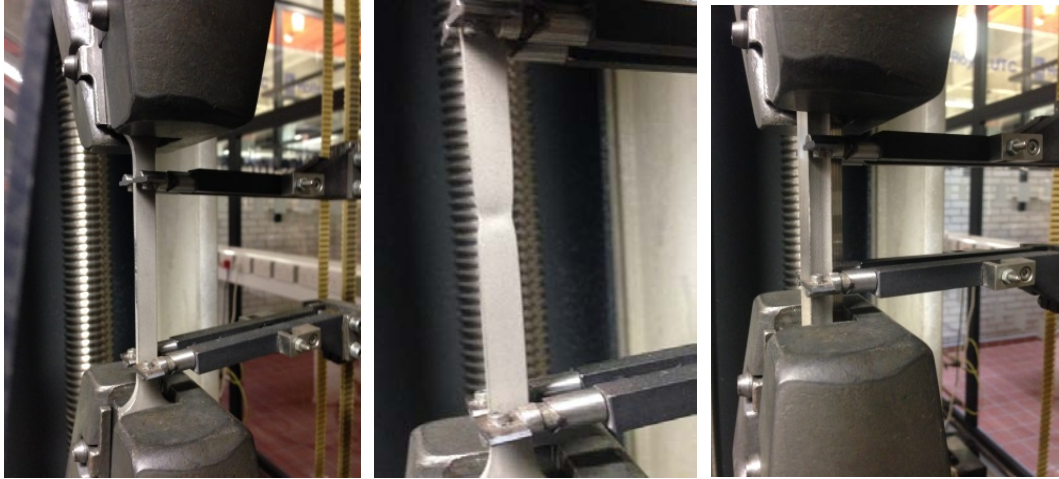
Fig. 2: Flat and corner material coupons tested in tension
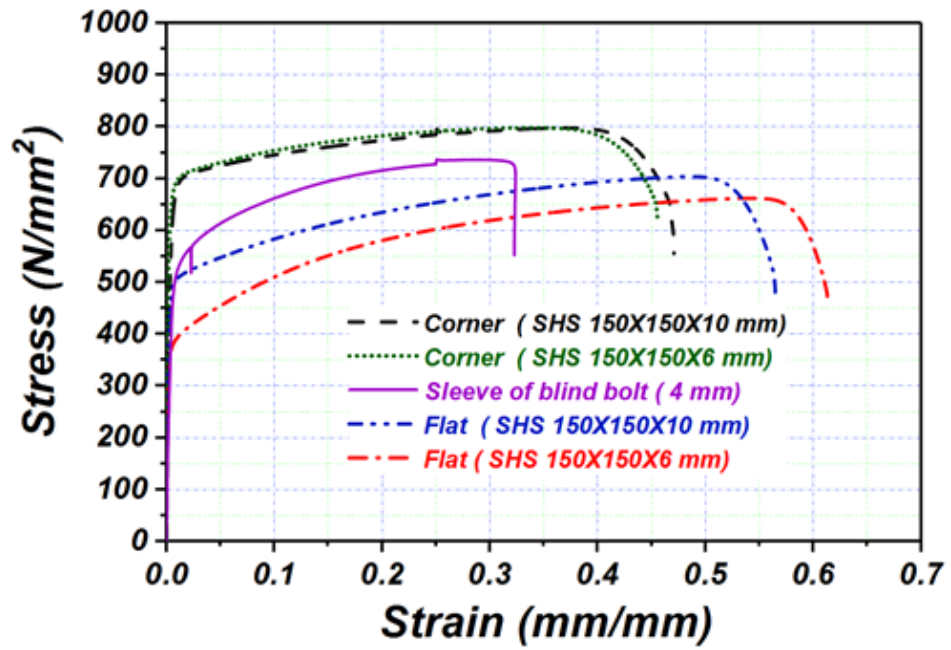
Fig. 3: Material response of Hollo-bolt sleeve and SHS
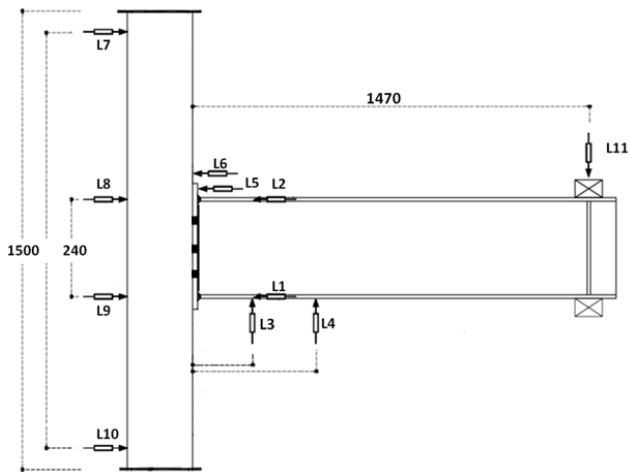
Fig. 4: General arrangement of experimental setup and instrumentation.
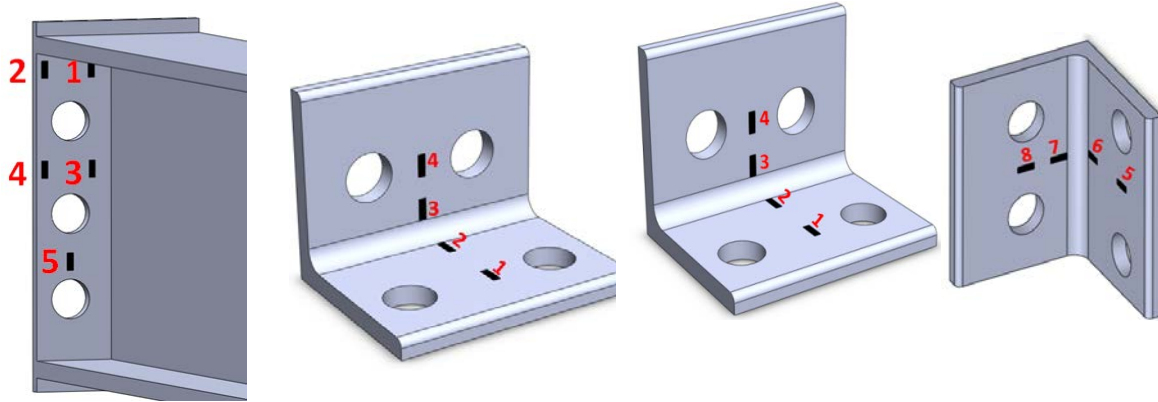
(a) FEP-1 & FEP-2   (b) TSAC-1 & TSAC-2   (c) TSWAC-1 & TSWAC-2

Fig. 5: Location and numbering of strain-gauges for each specimen
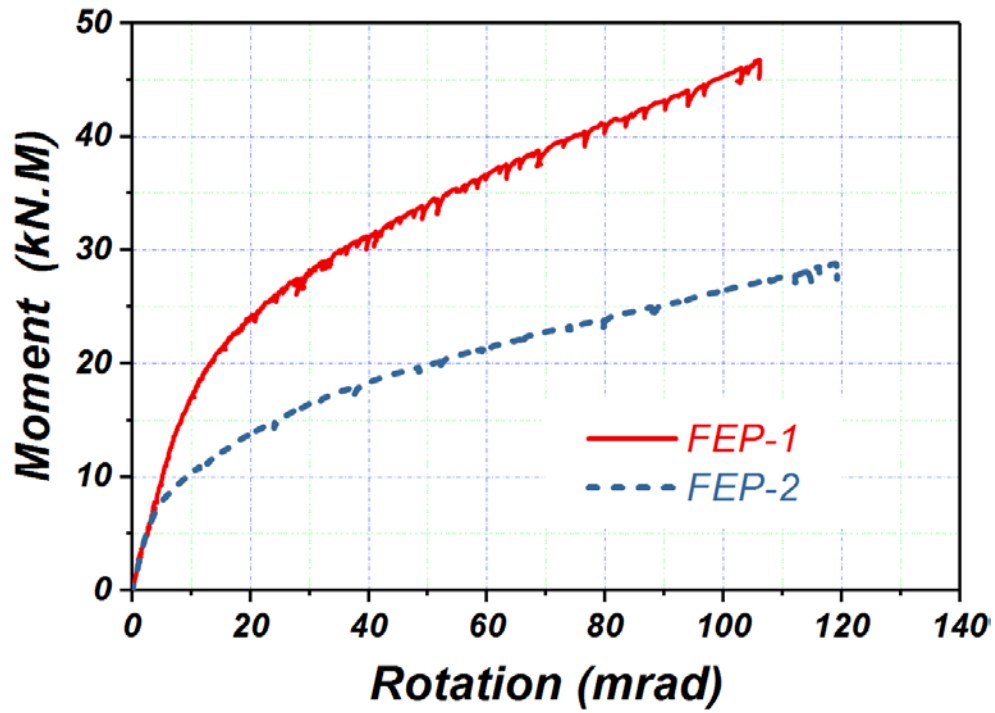
Fig. 6: Moment-rotation response for FEP-1 and FEP-2 specimens
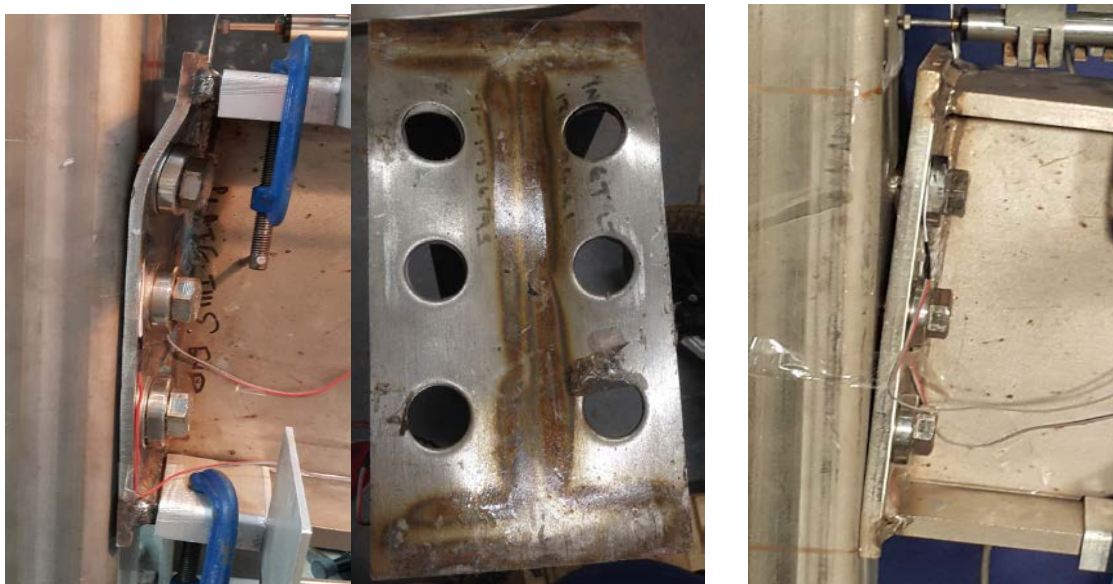
(a) FEP-1: plastic deformation of the end plate and closeup of the deformed end plate

(b) FEP-2: pull-out of top Hollo-bolts

Fig. 7: Failure modes of FEP-1 and FEP-2 specimens
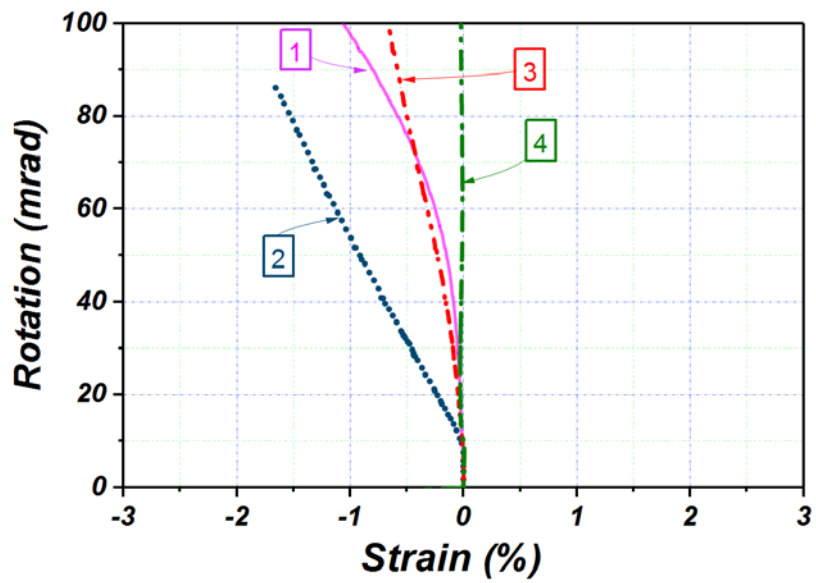
(a) Measured strains for FEP-1 specimen
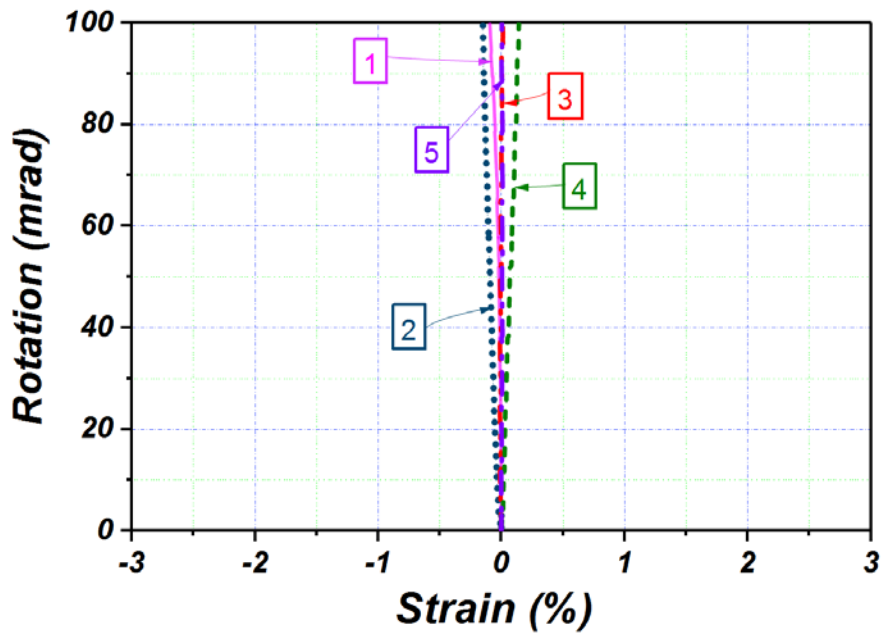
(b) Measured strains for EEP-2 specimen

Fig. 8: Strain evolution with increasing rotation for FEP specimens
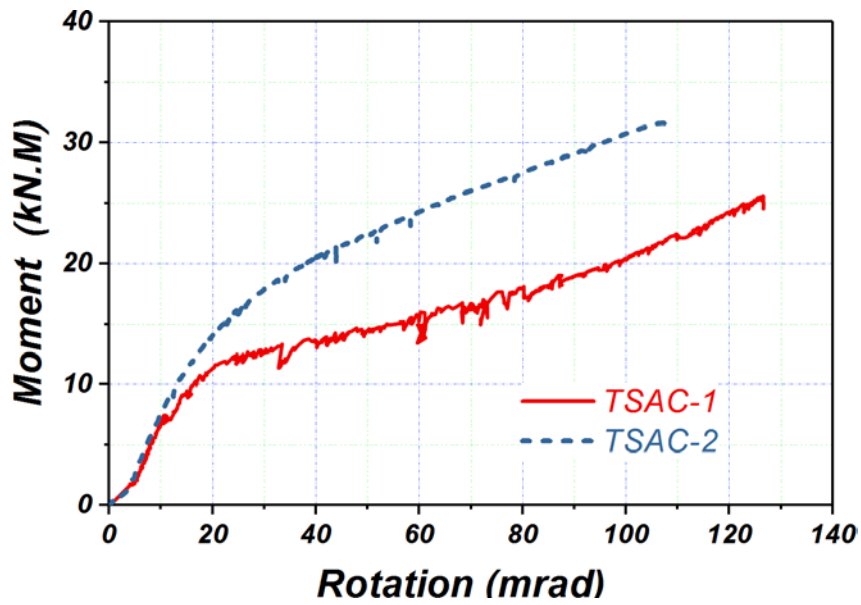
Fig. 9: Moment-rotation response for TSAC specimens

(a) TSAC-1: bending of top angle cleat

(b) TSAC-2: deformation of angle cleat, column face and sleeve Hollo-bolt

Fig. 10: Failure modes of TSAC specimens
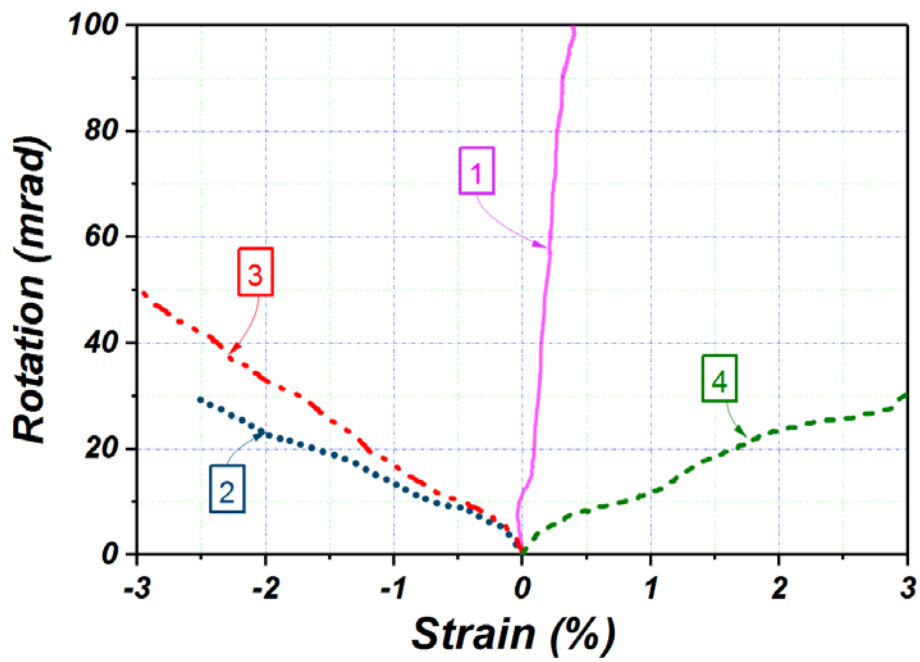
(a) Measured strains for TSAC-1 specimen
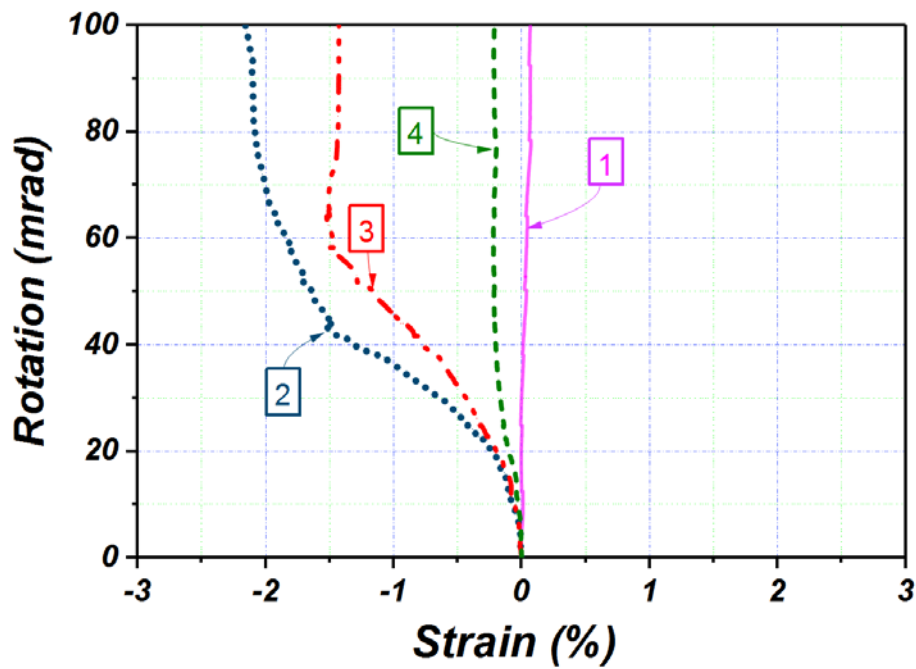
(b) Measured strains for TSAC-2 specimen

Fig. 11: Strain evolution with increasing rotation for TSAC specimens
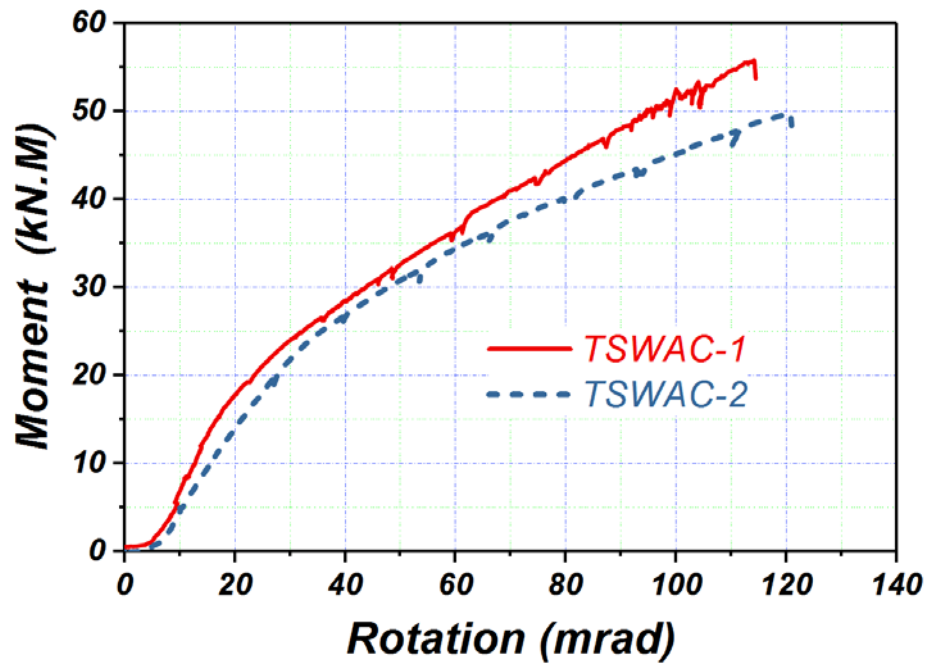
Fig. 12: Moment-rotation response for TSWAC specimens
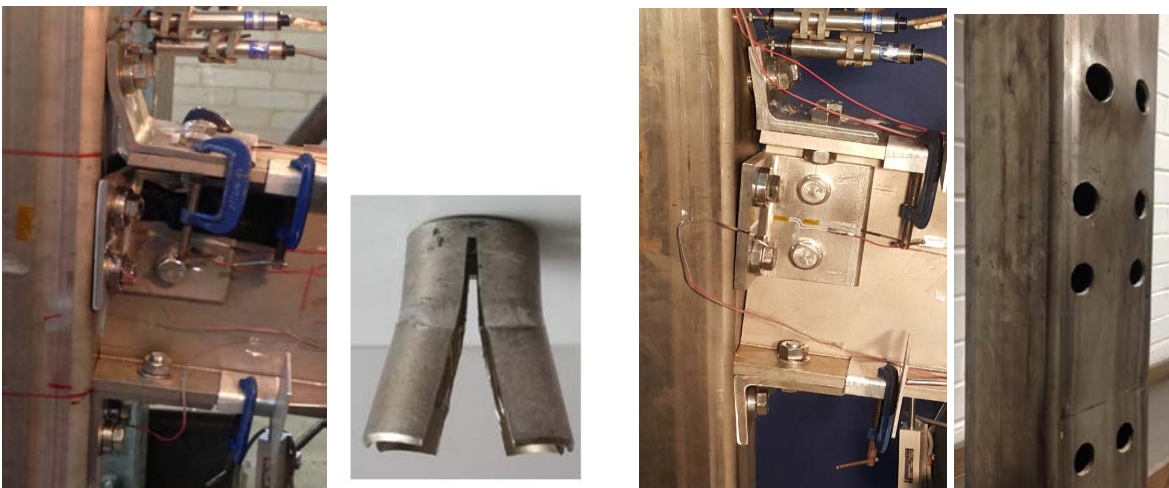
(a) TSWAC-1: bending of top angle cleat and indentation of the sleeve of the Hollo-bolt

(b) TSWAC-2: deformation of angle cleats, column face and Hollo-bolts

Fig. 13: Failure modes of TSWAC specimens
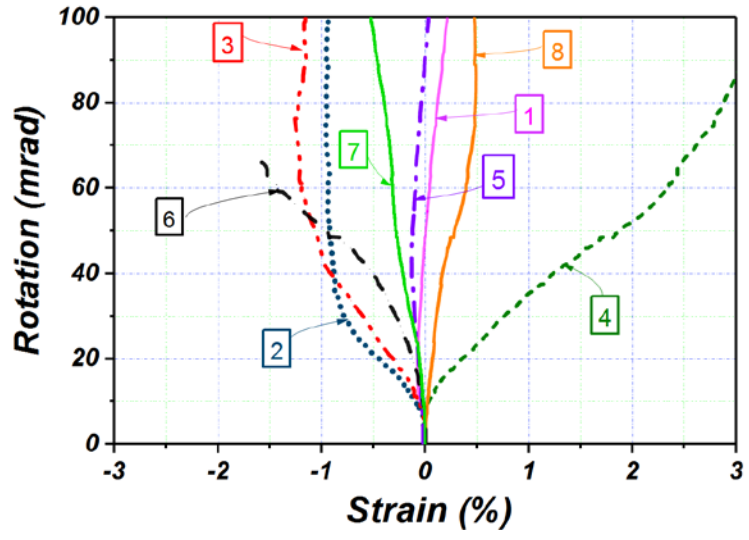
(a) Measured strain for TSWAC-1 specimen
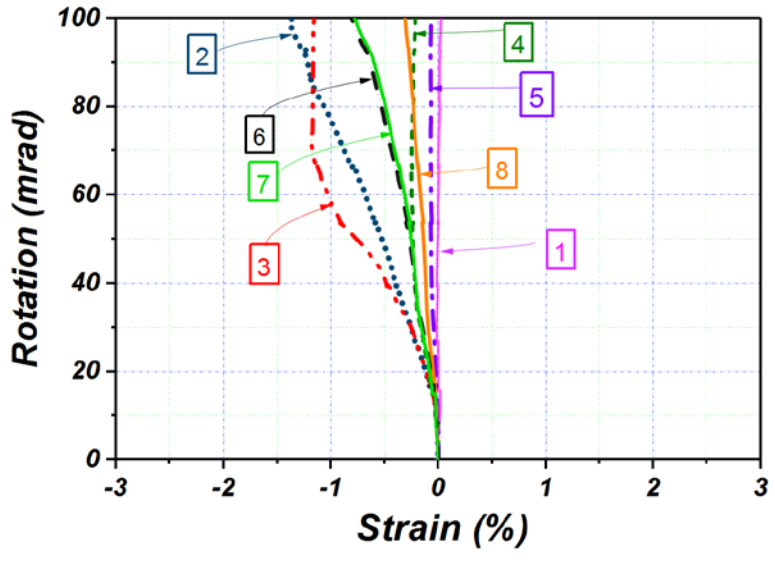
(b) Measured strain for TSWAC-2 specimen

Fig. 14: Strain evolution with increasing rotation for TSWAC specimens

a) Bolt Shank and head

b) Sleeve

c) Cone

d) Assembled Hollo-bolt
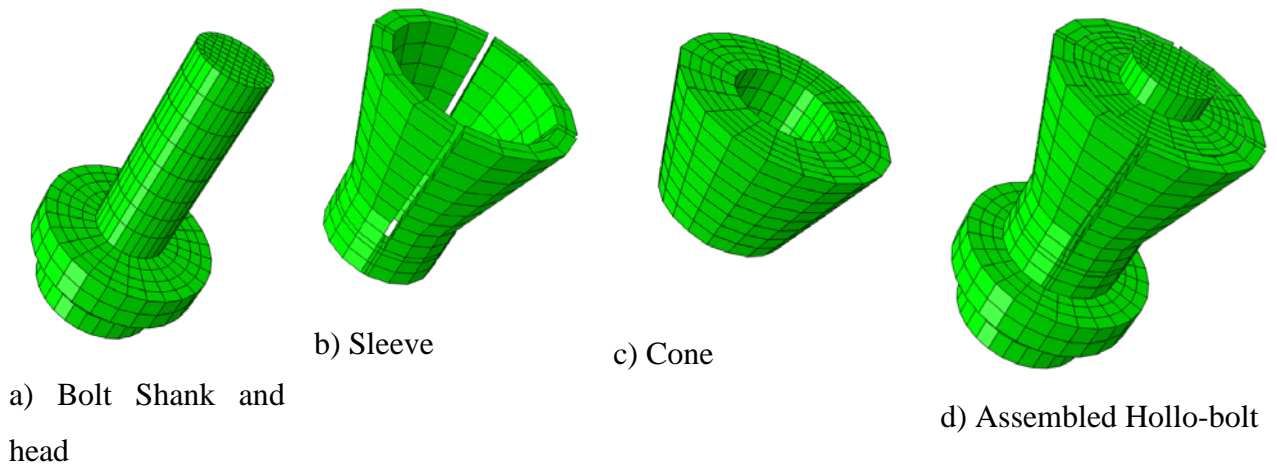
Fig. 15: Geometrical idealization and discretization of the Hollo-bolt

(a) FEP- 1

(b) FEP- 2

(c) TSAC-1

(d) TSAC-2

(e) TSWAC-1
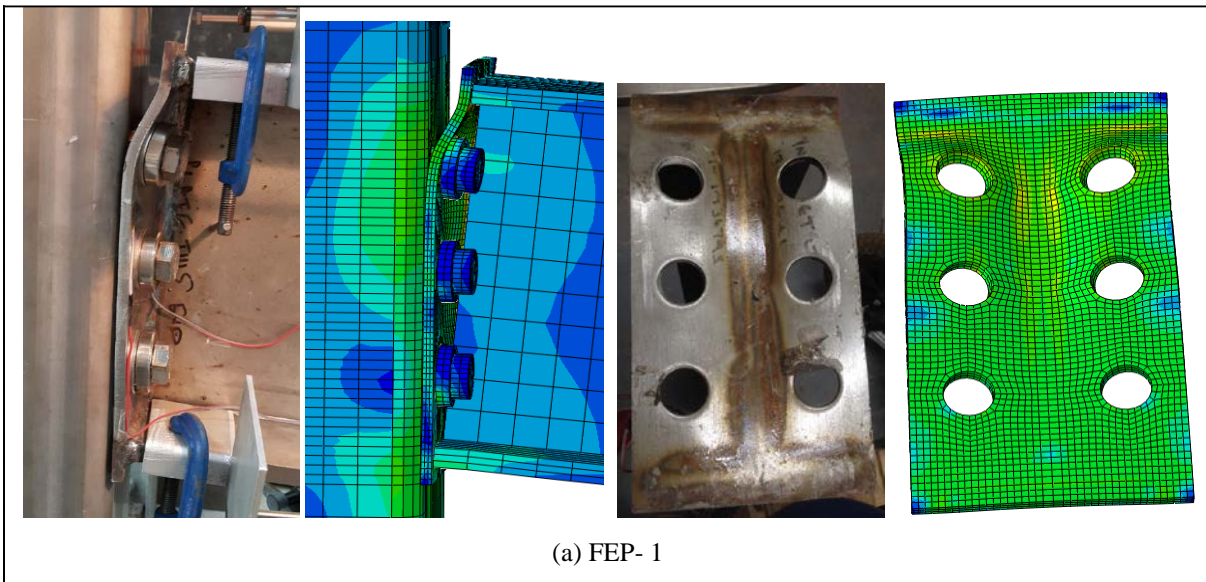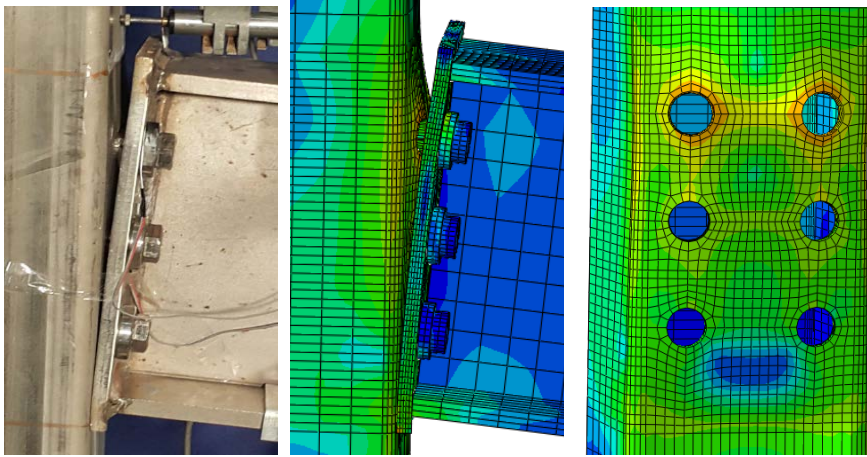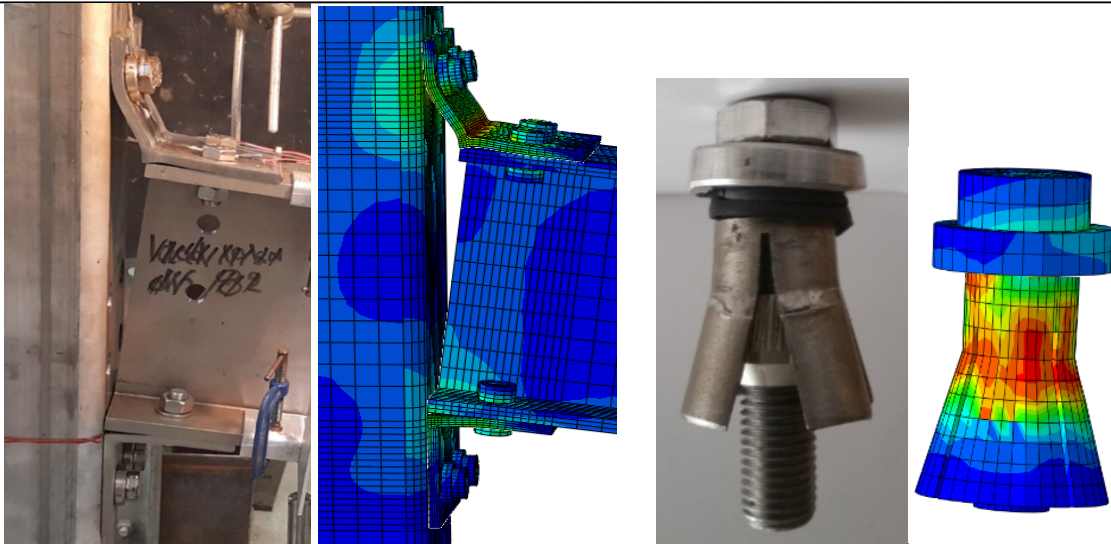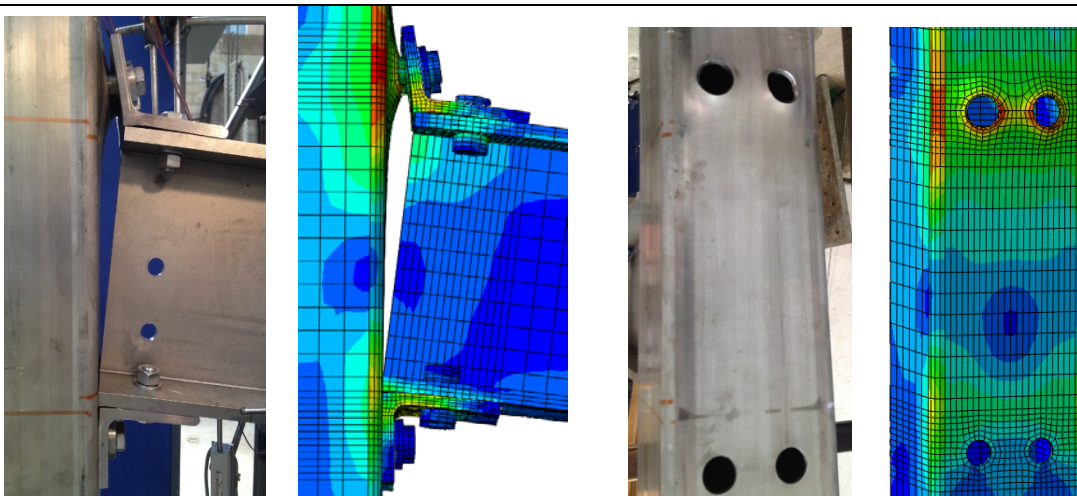
(f) TSWAC-2
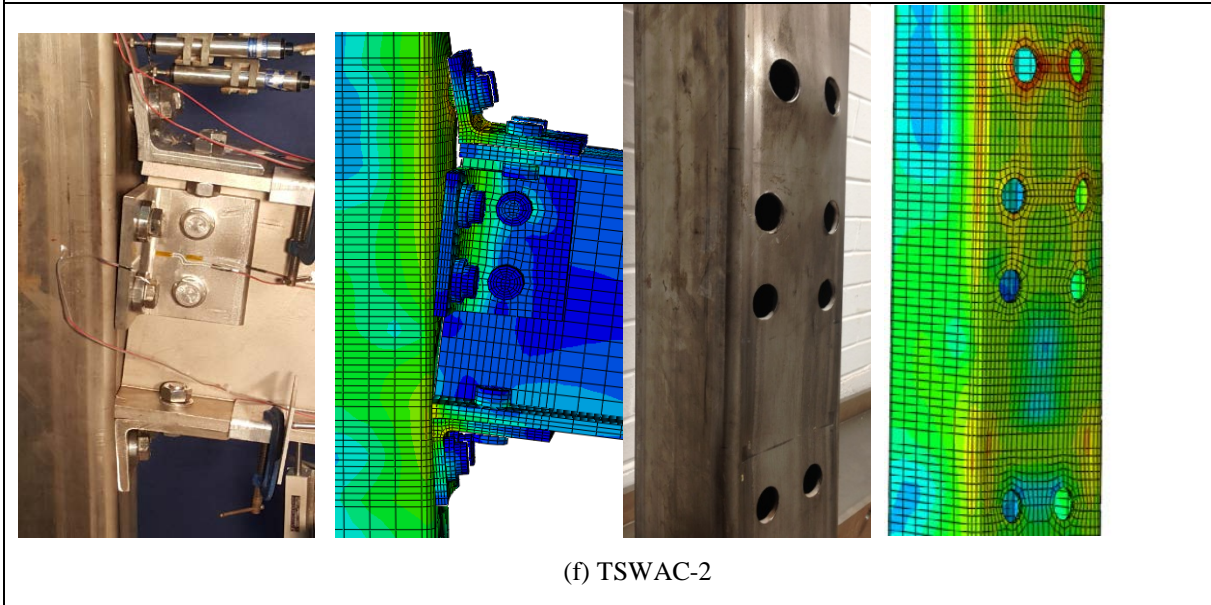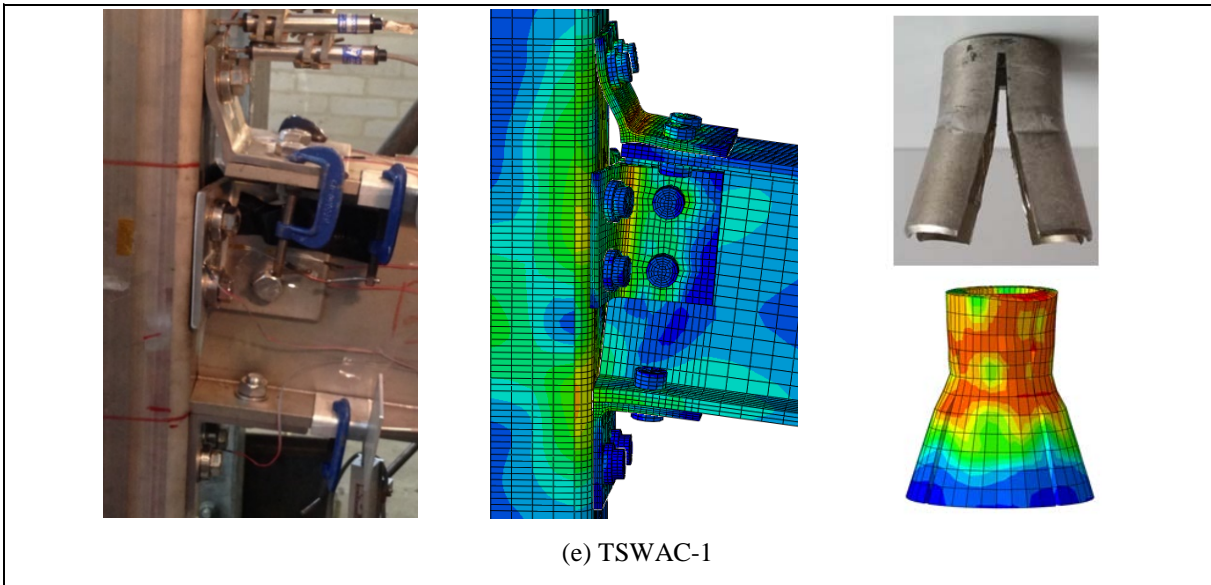
Fig. 16: Experimental and numerically obtained failure modes of tested joints.

a) FEP-1

b) FEP-2

c) TSAC-1

d) TSAC-2

e) TSWAC-1

f) TSWAC-2
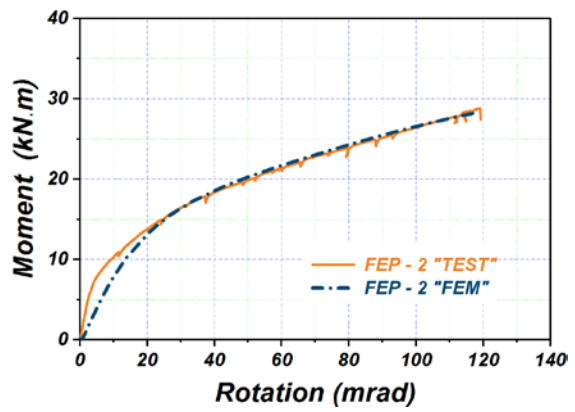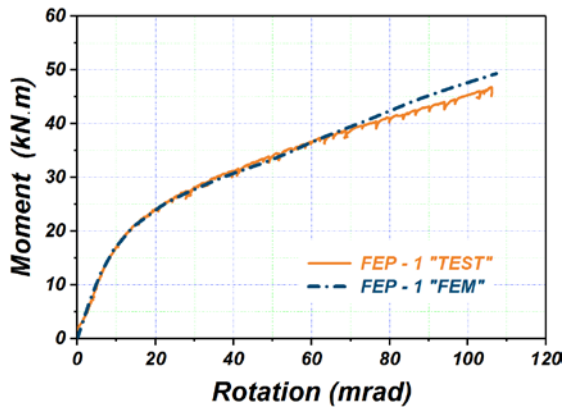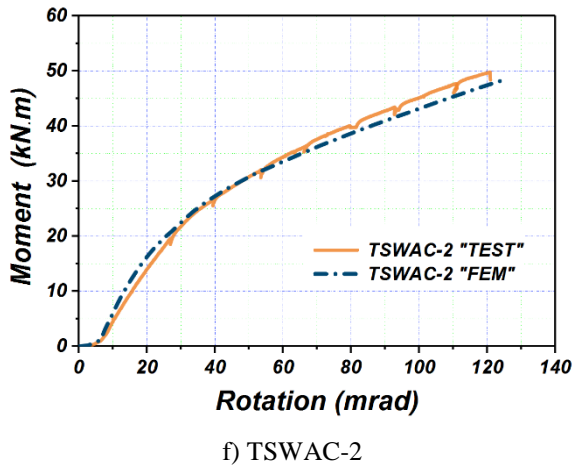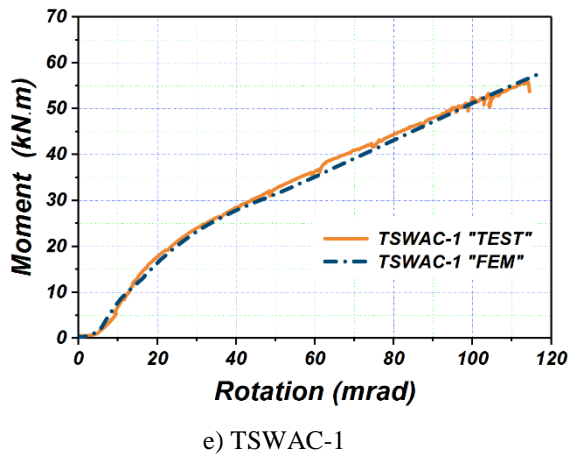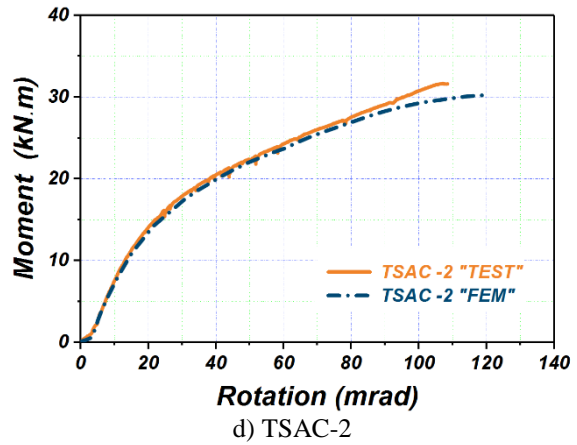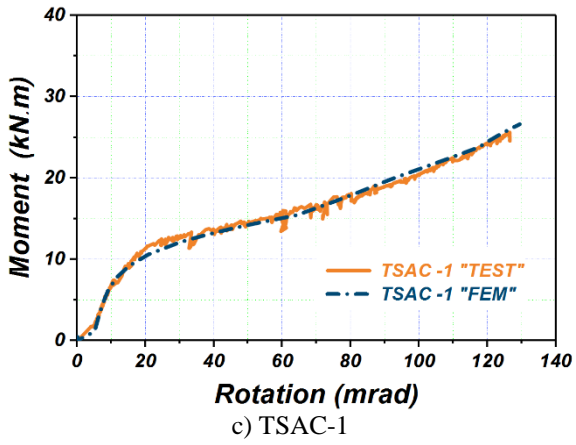
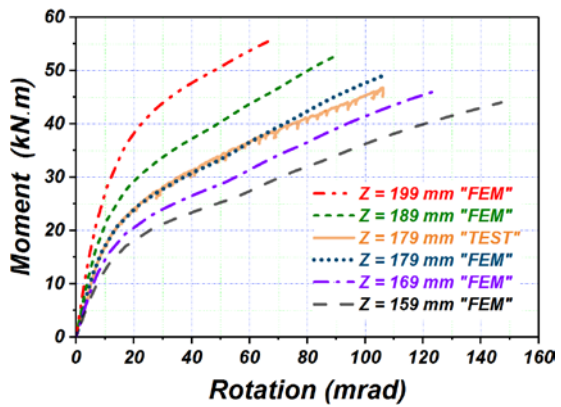Fig. 17: Experimental and numerical moment-rotation response of tested joints.
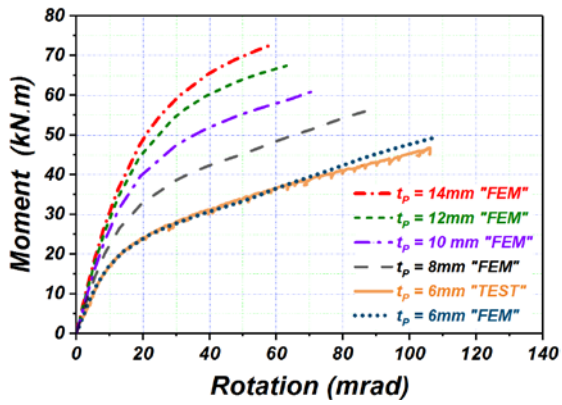
(a) M-Φ curves for different plate thicknesses t_p
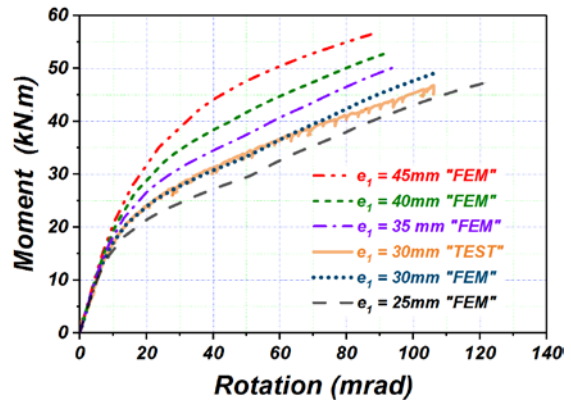
(b) M-Φ curves for different bolt edge distances e_2
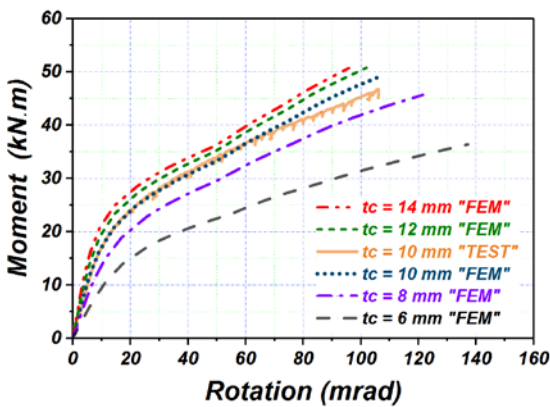
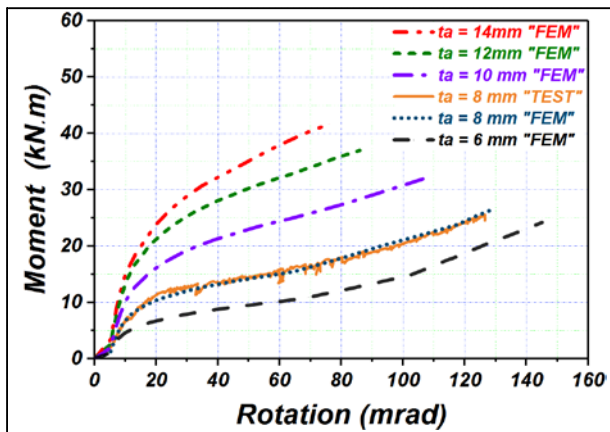(c) M-Φ curves for different column flange thicknesses tc
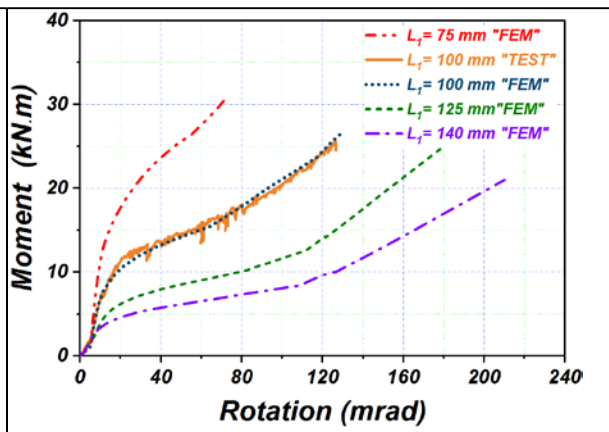
(d) M-Φ curves for different values of the lever arm z

Fig. 18: Parametric study for FEP connections

(a) M-Φ curves for different angle cleat thicknesses t_a

(b) M-Φ curves for different lengths L_1 of the connected angle cleats

(c) M-Φ curves for different column flange thicknesses t_c

(d) M-Φ curves for different bolt edge distances e_2

Fig. 19: Parametric study for TSAC connections

(a) M-Φ curves for different angle cleat thicknesses t_a

(b) M-Φ curves for different lengths L_1 of the connected angle cleats

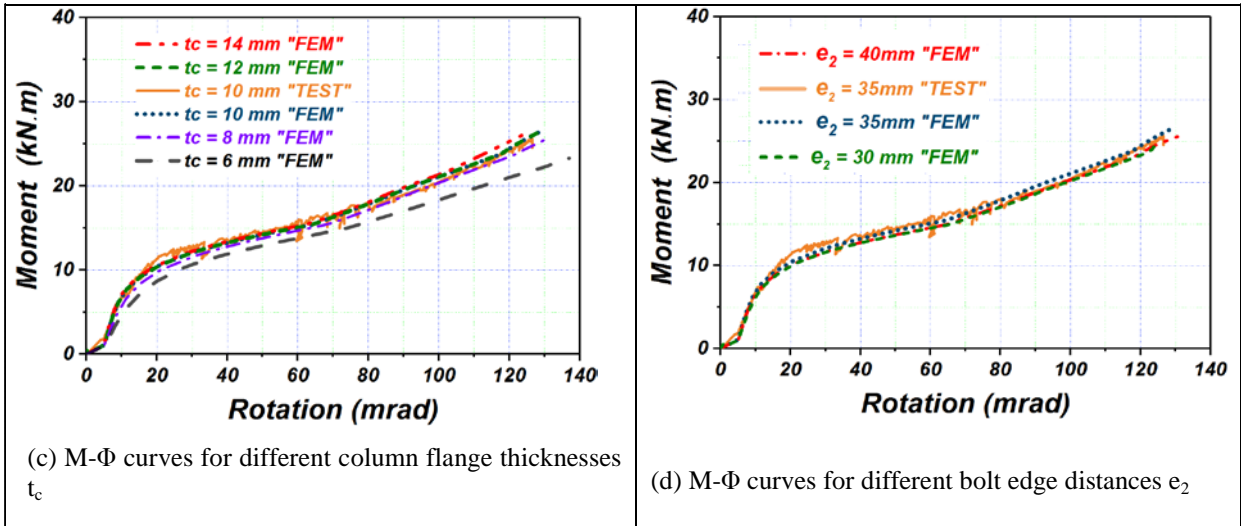(c) M-Φ curves for different column flange thicknesses t_c
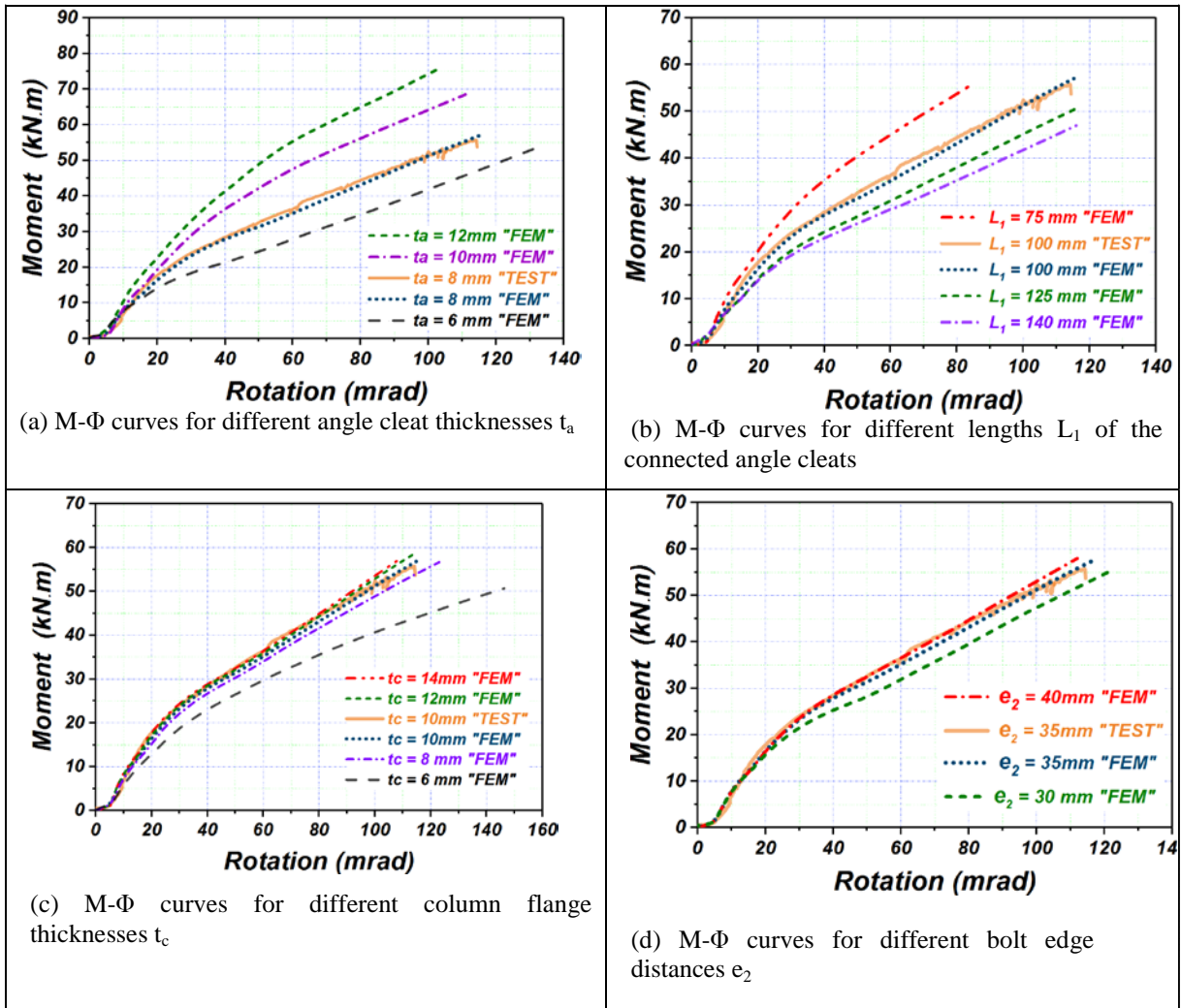
(d) M-Φ curves for different bolt edge distances e_2

Fig. 20: Parametric study for TSWAC connections